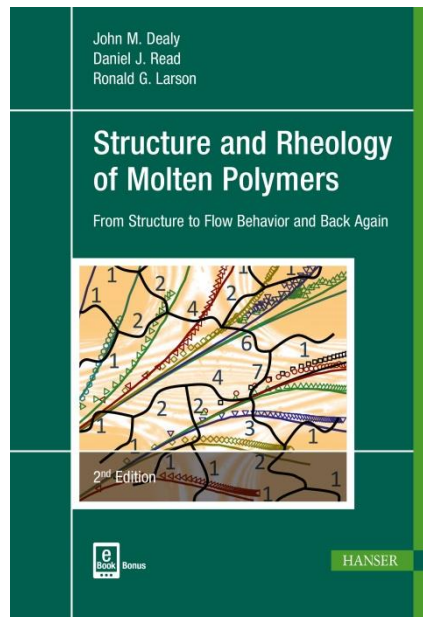# HANSER

Sample Pages

Structure and Rheology of Molten Polymers

John M. Dealy
Daniel J. Read
Ronald G. Larson

For further information and order see

www.hanserpublications.com (in the Americas)

www.hanser-fachbuch.de (outside the Americas)

Contents

Preface to the Second Edition

There have been many important developments in this field since the first edition of the book appeared over 10 years ago, and these are described in some detail in this new edition. Results of recently developed molecular models suggest the possibility of predicting the rheological behavior of a molten polymer when its molecular structure is well-known. Such models also provide the basis of methods for using rheological data to obtain information about the structure of a polymer whose structure is not known in detail. These models and relationships between structure and rheology are presented here from both phenomenological and molecular-theoretical points of view.

This book was designed for several types of reader. For those who have a basic knowledge of rheology but little experience with polymers, we provide in the early chapters sufficient information about polymer physics and chemistry for an understanding of the later chapters on the rheological behavior of melts. For readers who are currently active in polymer rheology and would like to know the state of the art with respect to quantitative relationships between molecular structure and rheology, the later chapters of the book provide this information. Thus, the book provides both an introduction to polymers and rheological concepts as well as an advanced treatment of potential interest both to polymer scientists and plastics engineers.

Until recent years, there existed major barriers to the development of quantitative relationships between the molecular structures of commercial polymers and their rheological behavior. Methods used to produce these materials yielded materials having complex and imprecisely controlled structures. The molecular weight distributions of linear polymers tended to be broad and somewhat irreproducible. And the branching structures of long-chain branched polymers, particularly low-density polyethylene, involve multidimensional distributions that can neither be predicted nor characterized with precision.

However, over the last 10 years, advances in the areas of catalysis and molecular modeling have changed this situation dramatically. Using single-site catalysts, it is possible to produce, on an industrial scale, polymers having structures that are much better defined and reproducible than those produced previously. Furthermore, recent advances in molecular models based on tube or slip-link concepts have made

it possible to predict the behavior of a widening range of molecular structures. While still requiring further work, particularly to deal with broad molecular weight distributions and complex branching structures, the new models are beginning to be used for the prediction of flow behavior of some commercial polymers. The objective of this book is to present these important developments, along with the background necessary to understand them, and to provide industrial and academic researchers with the up-to-date knowledge and expertise required to use them effectively.

It is not feasible to mention here all the people who have helped us in various ways during the several years we spent writing this book, but we would like to mention the following who were helpful in particularly important ways: Stéphane Costeux, Chinmay Das, Jeffrey Giacomin Jörg Läuger, Thomas Schweizer, João Soares, Manfred Wagner, and Manfred Wilhelm. And we must mention the support of our tolerant families and the patient guidance of our Editor, Mark Smith, who were essential for the completion of the project.

August 15, 2017

Montreal, Quebec
Leeds, England
Ann Arbor, Michigan

Preface to the First Edition

Results of recently developed molecular models suggest the possibility of predicting the rheological behavior of a molten polymer when its molecular structure is well-known. Such models also provide the basis of methods for using rheological data to obtain information about the structure of a polymer whose structure is not known in detail. These models and relationships between structure and rheology are presented here from both phenomenological and molecular-theoretical points of view.

This book is intended to be useful to several types of reader. For those who have a basic knowledge of rheology but little experience with polymers, we have provided in the early chapters sufficient information about polymer physics and chemistry for an understanding of the later chapters. For readers who are currently active in polymer rheology and would like to know the state of the art with respect to quantitative relationships between molecular structure and rheology, the later chapters of the book provide this information. Thus, the book provides both an introduction to polymers and rheological concepts as well as an advanced treatment of potential interest both to polymer scientists and plastics engineers.

Until recent years, there existed major barriers to the development of quantitative relationships between the molecular structure of molten polymers and their rheological behavior. First, reaction systems capable of producing polymers on an industrial scale yielded materials with complex and imprecisely controlled structures. Second, the molecular weight distributions of linear polymers tended to be broad and somewhat irreproducible. And, finally, the branching structure of long-chain branched polymers, particularly low-density polyethylene, involves multidimensional distributions that can neither be predicted nor characterized with precision.

However, over the last ten years, advances in the areas of catalysis and molecular modeling have changed this situation dramatically. Using single-site catalysts, it is now possible to produce on an industrial scale polymers having structures that are much better defined and reproducible than those produced previously. Furthermore, new molecular models, particularly those based on the concept of a "molecule in a tube", have been developed that can predict rheological behavior based on knowledge of molecular structure. While still requiring further work, particularly to deal

with broad molecular weight distributions and complex branching structures, the new models show great promise for the quantitative prediction of flow behavior of polymers of commercial importance. The objective of this book is to present these important developments, along with the background necessary to understand them, and to provide industrial and academic researchers with the up-to-date knowledge and expertise required to use them effectively.

It is not feasible to mention here all the people who have helped us in various ways during the several years we spent writing this book, but we would like to mention the following who were helpful in particularly important ways: Ralph Colby, Stéphane Costeux, Richard Graham, Willem de Groot, Teresa Karjala, David Lohse, Guiseppe Marrucci, Hiroshi Watanabe, and Paula Wood-Adams. And we cannot fail to mention that the support of our tolerant families and the patient guidance of our Hanser editor, Dr. Christine Strohm, were essential to the completion of the project.

September 29, 2005

Montreal, Quebec
Ann Arbor, Michigan

1 Introduction

■ 1.1 Melt Structure and Its Effect on Rheology

Our subject is how molecular structure affects melt flow and how rheological behavior can provide information about structure. Rheology has been used as a semiquantitative tool in polymer science and engineering for many years, for example for quality control, but quantitative relationships between structure and measurable properties were elusive, particularly in the case of commercial polymers. However, catalyst systems and synthesis methods have greatly improved our control of molecular structure. This, together with major advances in the modeling of rheological behavior, has brought us much closer to quantitative correlations between structure and rheology.

The relationship between the structure and the rheology of polymers is of practical interest for two reasons. First, rheological data are both very sensitive to certain aspects of the structure and easier to obtain than those of analytical methods such as gel permeation chromatography. Second, it is the rheological properties that govern the flow behavior of polymers when they are processed in the molten state.

When we speak of the structure of a polymer, we mean the size and shape of the molecules and the distributions of these characteristics among molecules. Thus, quantities of interest include molecular weight and its distribution, tacticity (when the monomer has a pseudochiral center), and branching (types, lengths, and their distributions). For linear homopolymers in which tacticity is not an issue, the molecular weight distribution contains complete information regarding structure. This is not a trivial special case, as it includes linear polyolefins that are used in many applications ranging from blow-molded milk bottles to molded polycarbonate compact disks. And even for such relatively simple materials, rheology provides a valuable tool for polymer characterization. Obviously, the determination of the structure of branched polymers is more complex.

■ 1.2 Overview of This Book

We treat here only systems in which most of the molecules are of a sufficient length to be in a highly entangled state. The basic idea of "entanglement" is that polymer molecules in a melt are embedded in a sea of other very long molecules, and this greatly restricts their motion in response to an imposed deformation or stress. Solutions of polymers in which the concentration and molecular weight are sufficient to generate a strong entanglement effect are also governed by the relationships discussed here and are mentioned from time to time. Immiscible blends are not treated, because their rheological behavior is strongly affected by interfacial tension. Neither do we deal with filled polymer systems; useful treatments of the rheological behavior of these materials are available [1–3].

Most of the data shown are for polyolefins and vinyl polymers, because these are the materials that are most commonly met with in a highly entangled state. They can be easily polymerized at high molecular weights (that is, molecular weights above 10,000), and their entanglement molecular weights are sufficiently low that the products are highly entangled. In addition, polymers in these categories, particularly polyethylene, polypropylene, and polystyrene, are the world's most important commercial polymers and are generally very highly entangled.

Chapter 2 describes quantitative, nonrheological methods for determining molecular structure. But all characterization methods are limited in what they can tell us about structure in the absence of any information about how a sample was polymerized. Chapter 3 surveys the types of reaction systems used in polymerization and describes the molecular structures that can be produced by each. Anionic and living free-radical polymerizations are used in the laboratory to prepare samples having ideal structures, while processes used in industry produce materials that more complex in structure. The development of single-site catalysts has led to the commercial production of polymers that, while they do not have the homogeneity of model polymers, do have structures that are reproducible and simply described.

Chapter 4 introduces the subject of linear viscoelasticity for readers new to rheology and also defines a number of terms that are used in the remainder of the book. The relaxation spectrum is introduced as well as methods for its measurement. Also, time-temperature superposition and its application are explained.

Chapter 5 contains a detailed discussion of the linear viscoelastic behavior of polymer melts. The most-often-used linear properties are the zero-shear viscosity and the storage and loss moduli; the effects of molecular weight, molecular weight distribution, and branching on these properties are described. While the approach is primarily phenomenological, melt behavior is interpreted qualitatively in terms of the molecular models that are presented in mathematical detail in later chapters.

Chapter 6 treats mean-field theories of melt behavior. We begin with the Rouse model for molecules in dilute solution and its modification by Bueche to deal with unentangled melts. The longest Rouse relaxation time emerges from this treatment and plays an important role in all molecular models. The tube model is introduced, in which the basic relaxation mechanisms involved in linear viscoelastic behavior are assumed to be "equilibration" among segments of the molecule within in a "tube" formed by surrounding molecules, and "reptation" out of this tube. The large difference between the time scales for these two processes explains the prominent plateau in the relaxation modulus of a monodisperse, entangled melt. In a polydisperse melt, short molecules cause the tube to become less restrictive of lateral motion during the reptation process, and this eliminates the flat plateau in the relaxation modulus. The slip link concept is an alternative to the tube picture, and models based on it are presented.

Chapter 7 describes the physics of the tube model in more detail and presents alternative approaches to dealing with polydispersity.

In Chapter 8, methods for inferring the molecular weight distribution of a linear polymer from rheological data are presented and compared. These range from semiempirical methods based on measurement of the viscosity as a function of shear rate to sophisticated techniques based on the molecular models presented in Chapters 6 and 7.

Chapter 9 presents tube models for linear viscoelasticity in systems with long-chain branching. Reptation of the molecule as a whole is suppressed by branch points, and relaxation takes place primarily by primitive path fluctuation, a relatively slow process.

Chapter 10 deals with nonlinear viscoelasticity primarily from a phenomenological point of view. Nonlinear behavior provides structural information that supplements that available from linear data, particularly in the case of long-chain branched polymers. Stress relaxation after large step strain reveals a new feature that is described in terms of the "damping function," and it is explained by tube models as the result of retraction following chain stretch. Nonzero normal stress differences are nonlinear phenomena that occur in all large, rapid shearing deformations. In order to explain the effect of shear rate on the viscosity, the concept of "convective constraint release" is introduced into the tube picture. Except for step strain, shearing deformations do not generate significant chain stretch, but uniaxial (simple) extension does, and thereby displays interesting new phenomena such as "strain hardening," which has been found to be particularly useful in the detection of long-chain branching.

Tube models capable of describing the essential features of nonlinear behavior are described in Chapter 11, which also introduces constitutive equations based on tube models. Such equations are of practical importance, as they aim to predict the way a melt behaves during industrial forming operations.

Chapter 12 briefly summarizes the book and lists remaining challenges.

■ 1.3 Applications of the Information Presented

The recent developments mentioned above open the door to the development of quantitative models relating molecular structure to rheological behavior. The two direct applications of these models are the prediction of rheological behavior when the molecular structure is known and the determination of key aspects of molecular structure by means of rheological measurements. Going beyond the scope of this book, the relationship between melt structure and rheology is one link in a chain of relationships that starts from reaction conditions and ends in the way polymers behave in industrial melt-forming operations. Making use of developments in the modeling of polymerization reactions and of melt forming operations, one can imagine a not very distant future in which it will be possible to do the following steps:

1. Predict the detailed structure of a polymer given the monomer(s) catalyst system and reaction conditions used to prepare it.
2. Given its structure, predict the rheological behavior of a polymer using molecular models.
3. Invert the above process by using rheology to determine polymer structure, or to confirm the predictions of structure that were made based on Step 1 above.
4. Using numerical flow simulations, predict the detailed behavior of a polymer during processing based on predicted rheological properties.

There have been major advances in each item in this list in recent years, and one can imagine a future when it is possible to predict *a priori* the reaction conditions required to produce a polymer having a prescribed melt processing behavior. This book simply summarizes what is known about Step 1 of this chain, but provides a more thorough treatment of Step 2, and to the extent currently possible, Step 3. The book contributes also to Step 4 by describing rheological constitutive equations that might be used in the simulation of flows and stresses in polymer processing operations.

■ 1.4 Supplementary Sources of Information

We mention here some books for readers looking for more information on particular topics. The book by Ferry [4] continues to be a classic source in the area of polymer rheology, in spite of the fact that the third edition is now more than 35 years old. More recent but less encyclopedic books on rheology include those of Macosko [5], Morrison [6], and Münstedt and Schwarzl [7]. Dealy and Wang [8] deal with applica-

■ 2.3 Tacticity

The presence of any pendant group, even if it is only a methyl group, has an important effect on the crystallinity of a polymer. A polymer that has many such groups has a property called *tacticity*, which describes the distribution of orientations of side-groups along the chain. There are three types of distribution: *isotactic*, *syndiotactic*, and *atactic*. The simplest example is polypropylene, which can be polymerized in forms having all three tacticities. In isotactic polypropylene (i-PP), all the ethyl groups are on the same side of the chain, while the syndiotactic polymer (s-PP) has these groups on alternating sides. These two structures are sketched in Fig. 2.3. Of course, the actual molecule is not planar, so the sketch is, in fact, a projection of the molecule onto a plane. While the carbons in the backbone that are attached to the pendant groups are chiral centers, polypropylene does not have optical activity, because the atoms adjacent to it are also carbons.
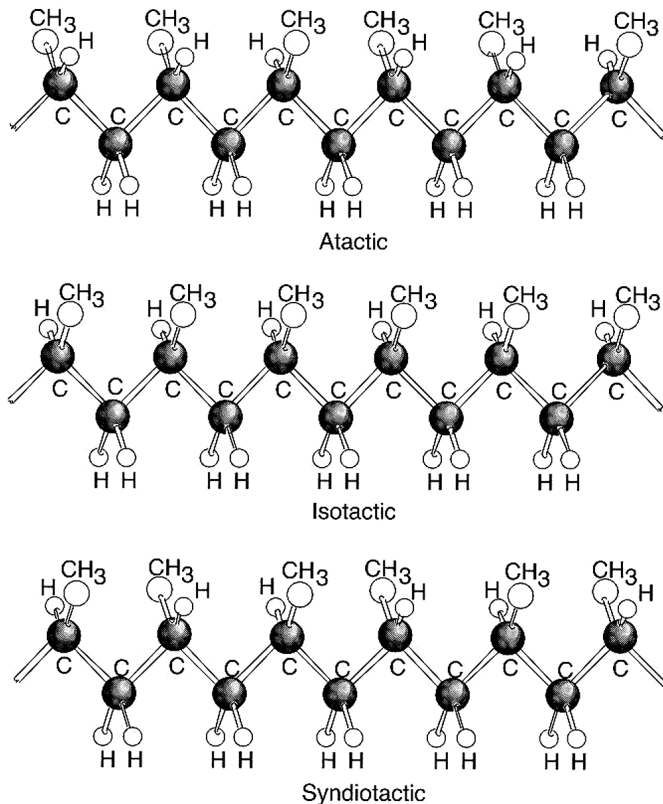
Figure 2.3 Sketch of projections onto the plane of atactic, isotactic and syndiotactic polypropylene molecules. The latter two are crystallizable, whereas the atactic isomer does not crystallize.

In a perfectly random, atactic polymer, the position of pendant groups varies randomly along the chain. Such a random distribution is said to be Bernoullian or a zero-order Markov chain. There are also intermediate structures, such as hemiisotactic and isotactic stereoblock polymers, which have randomly occurring, short runs of isotactic or syndiotactic structures. A detailed explanation of tacticity is given by Koenig [33]. Isotactic and syndiotactic polymers can crystallize, while atactic polymers cannot. Polymers other than polypropylene that have tacticity include polystyrene, poly(vinyl chloride), and poly(methyl methacrylate). Thus there are crystalline and non-crystalline forms of these polymers.

Tacticity can affect important physical properties such as the intrinsic viscosity and thus must be taken into account in characterization methods such as gel permeation chromatography. Jones et al. [34] used small-angle neutron scattering to study the chain dimension of syndiotactic polypropylene and found that the s-PP chain is substantially larger than that of i-PP. This implies that the s-PP molecule is stiffer than that of i-PP, which results in significant differences in the rheological and thermodynamic behavior of the two forms [34, 35]. The effect of tacticity on rheological properties is discussed in Chapter 5.

■ 2.4 Branching

The copolymerization of a higher α-olefin comonomer with polyethylene yields a polymer having short side-branches; for example the use of butene introduces ethyl branches. However, these short branches do not have an important effect on rheological properties such as viscosity. Much longer branches, on the other hand, have dramatic effects on rheological behavior [36]. Adding long-chain branches, while keeping the molecule weight constant, reduces the size of a molecule. As is explained in Section 5.10, this results in a reduction in viscosity at low molecular weight but an increase in viscosity at high MW. This is of great practical importance, as it provides a mechanism for altering the flow behavior of a polymer without affecting its crystallinity. For example, adding long-chain branches to a copolymer such as LLDPE makes it possible to control, independently, the flow behavior and the crystallinity.

There are three general types of fairly well-defined branching structures: stars, combs and randomly branched polymers (see Fig. 2.4). In addition, systems of any degree of complexity can be produced. A hyperbranched polymer (HBP) is randomly branched and has a complex structure in which there are branches on branches. In general, such a system has broad distributions of molecular weight and branching structure. An idealized model for a hyperbranched polymer is the n-Cayley tree. This is a structure in which each branch point, or vertex, has n branches, and this struc-

Star   H-Molecule   Comb

Dendrimer   Cayley tree
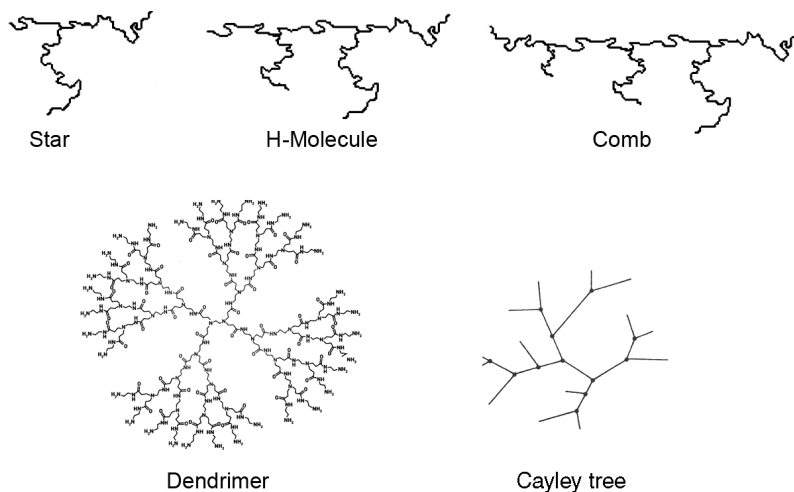
Figure 2.4 Sketches illustrating various branched structures: star, H-polymer, dense comb, Cayley tree, and dendrimer.

ture is propagated through multiple generations. A dendrimer is a highly-branched, monodisperse, symmetrical molecule built up from a multifunctional core by adding monomer layers in a stepwise fashion. The shape of the molecule becomes more and more spherical until steric hindrance prevents further symmetrical growth. Dendrimers must be made under very precisely controlled conditions to ensure the orderly build-up of the molecule. A dendrimer is a special case of a hyperbranched polymer. The branching structures mentioned above are illustrated in Fig. 2.4.

Long-chain branching greatly complicates the characterization and description of molecular structure. It is possible, by painstaking procedures, to prepare samples having reasonably uniform branching structures such as stars and combs [37]. But branched commercial polymers are usually randomly branched and may have complex structures in which there are distributions of backbone lengths, branch lengths, branch point locations and branching complexity. In fact, even the identification of a *backbone* is problematic when there are branches on branches. Low-density polyethylene (LDPE), made by a high-pressure, free-radical process, is an example of an important commercial material with a complex branching structure.

A parameter that describes the level of branching in a mainly linear polymer is the branching frequency λ, which is the average number of branch points per 1000 backbone carbon atoms. This is related to the average number of branch points per molecule β and the number average molecular weight, M_n. For polyethylene this is:

$$\lambda = \frac{\beta\,(14)\,(1000)}{M_n} \tag{2.74}$$

■ 2.5 Intrinsic Viscosity

2.5.1 Introduction

The oldest, simplest and most widely used method for obtaining information about molecular weight is based on measurement of the viscosity of a dilute solution. We will see that this quantity is less sensitive to molecular weight than the zero-shear viscosity of the melt. However, the apparatus required is much simpler and can be used in combination with GPC to determine molecular weight distribution. Furthermore, it is often impossible using a commercial rheometer to determine the zero-shear viscosity of a melt. Kulicke and Clasen [38] provide additional information regarding intrinsic viscosity.

Several quantities are used to describe the low-shear-rate limiting viscosity of a solution η in terms of the viscosity of the solvent, η_s, and the concentration of polymer, c. These are defined as follows.

The relative viscosity (viscosity ratio): $\eta_{rel} \equiv \eta/\eta_s$

The specific viscosity: $\eta_{sp} \equiv \eta_{rel} - 1 = \eta/\eta_s - 1 = (\eta - \eta_s)/\eta_s$

The reduced viscosity (viscosity number): $\eta_{red} \equiv \eta_{sp}/c$

The inherent viscosity: $\eta_{inh} \equiv (\ln \eta_{rel})/c$

The intrinsic viscosity: $[\eta] \equiv \lim_{c \to 0}\left(\dfrac{\eta_{sp}}{c}\right) = \lim_{c \to 0}(\eta_{red}) = \lim_{c \to 0}(\eta_{inh})$ (2.75)

The units for c (concentration) in all these definitions are g/cm^3, and those for $[\eta]$ are thus cm^3/g.

Because it is evaluated in the limit of infinite dilution, the intrinsic viscosity provides information about the average size of molecules in a solution in which there is no interaction between molecules. In practice, for a linear, monodisperse polymer, the relationship used to calculate the molecular weight from the intrinsic viscosity is the one proposed by Mark [39], Houwink [40], and Sakurada [41] and given here as Eq. 2.76.

$$[\eta] = K_m \, M^a$$ (2.76)

where the empirical constants K_m and a depend on the polymer, the solvent and the temperature. We will call this the MHS equation and describe its use in detail in Section 2.5.4. However, because the intrinsic viscosity is so widely used, and because this book is concerned primarily with molecular structure, it is important to

■ 3.4 Living Polymers Having Prescribed Structures

In order to test molecular dynamics models and empirical correlations, it is necessary to synthesize polymers having precisely controlled molecular structures [9]. Such "model polymers" were for many years *living polymers* made in reactions with negligible termination or chain transfer. Termination halts the growth of a chain, while chain transfer terminates one chain but simultaneously generates a new radical. Thus, active centers are never lost, and polymerization continues until all the monomer is depleted. If more monomer is then added, the reaction continues, and if a different monomer is added, a block copolymer is produced. Such living polymers are made by chain reactions of monomers containing a double bond. A more recently developed technique is free-radical (*living/controlled*) polymerization, which is described in Section 3.4.2. (IUPAC has adopted the term "reversible deactivation radical polymerization" (RDRP) for this process.) This process is much simpler than true living polymerization, but the products are not as homogeneous.

In a living polymer, the number-average molecular weight is simply the grams of monomer present initially per mole of initiator. An ideal living polymer has a molecular weight distribution described by the Poisson distribution (given in Chapter 2). The polydispersity index (M_w/M_n) corresponding to a Poisson molecular weight distribution is given by:

$$PI = 1 + \frac{M_0}{M_n} - \left(\frac{M_0}{M_n} \right)^2 \tag{3.1}$$

where M_0 is the molecular weight of the monomer. For high molecular weights, $M_n \gg M_0$, the polydispersity approaches unity in accord with the following approximation that is valid near the limit of monodispersity:

$$\frac{M_w}{M_n} = 1 + \frac{M_0}{M_n} = 1 + \frac{1}{P_n} \tag{3.2}$$

where P_n is the number-average degree of polymerization. In fact, it is not possible to produce a polymer in which every molecule has exactly the same mass, but if P_n and the ratio of the rate of propagation to the rate of initiation are small, very narrow distributions can be produced. For example, Gold [14] calculated that when this ratio is 0.1, the polydispersity is 1.008, and when it is 10, the polydispersity is still only 1.019.

With the exception of a few commercial polymers such as polyisobutylene, polybutadiene and styrene-butadiene block copolymers, living polymers are prepared in small quantities under stringent conditions. Larger amounts can only be prepared by

repeating the synthesis many times, and this is a costly and time-consuming process. In the case of hydrogenated polybutadiene, used to prepare samples that resemble polyethylene, the need for the secondary hydrogenation step renders the process even more costly. This has so far limited the extent to which it has been possible to use these materials. Gell et al. [15] prepared asymmetric stars with structures similar to ethylene-propylene copolymers by hydrogenation of star-branched polyisoprene. The reactions to produce these materials took up to three weeks, and fractionation was required to remove by-products. While a single linear viscoelastic characterization at one temperature can be completed with a few grams, it is necessary to repeat tests a number of times in order to establish the precision of data. And for studies of nonlinear viscoelastic behavior, even larger samples are needed.

It is important to keep in mind that it is not possible to synthesize samples that are perfectly homogeneous in size and structure. Even for linear molecules, there is always a distribution of molecular weights. For example, Fig. 3.1 shows molecular weight distributions for ideal living polymers calculated using Eq. 2.72. We note that even for these low values of the polydispersity index (M_w/M_n = 1.005 and 1.001), there are still significant numbers of molecules having molecular weights much larger and smaller than the mean.
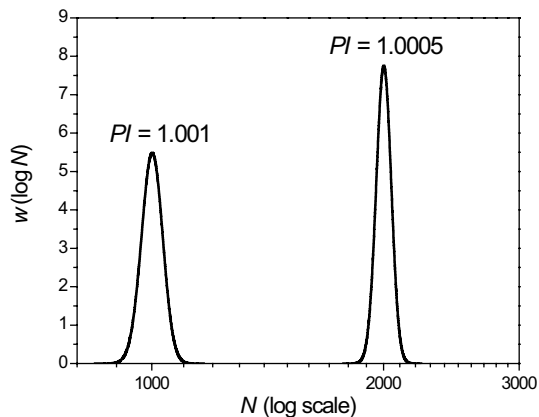
Figure 3.1 Molecular weight distributions in terms of degree of polymerization N according to the Poisson function (Eq. 2.72, in which $r_n = N$) for M_w/M_n = 1.001 and 0.005. The number-average degrees of polymerization are 1000 and 2000, respectively. Even these very narrow distributions include many molecules smaller or longer than average.

3.4.1 Anionic Polymerization

Anionic polymerization is a versatile technique widely used in polymer research [10, 11]. The key elements in making a living polymer by anionic polymerization are rapid initiation, so that all chains begin growing nearly simultaneously; elimination of chain transfer by reaction at a low temperature; and suppression of termination by the rigorous exclusion of impurities, particularly water and oxygen. In practice, it is impossible to eliminate all traces of termination agents, but one can achieve polydispersity indexes (M_w/M_n) of less than 1.01.

By means of anionic polymerization, it is also possible to produce polymers having many types of branching such as multi-armed stars and combs. Anionic polymerization has been used, for example, to make polystyrene, polybutadiene, and polyisoprene. An example of the anionic polymerization of a branched polymer is the technique of Roovers and Toporowski [16] for making comb polystyrenes. The model branched polymers that can be produced by means of block copolymerization and coupling chemistries include stars, H-shaped molecules and combs of various types [9]. So-called pom-pom polymers are of special interest, because their rheological behavior has been modeled by McLeish and Larson [17]. These molecules have several arms at each end of a central crossbar, and polybutadienes having this structure have been studied [18, 19].

Substituent groups on the double bond must stabilize the negative charge that develops in the transition state for the monomer addition step. They must also be stable to reactive anionic chain ends. Monomers that can be polymerized anionically include vinyl, diene, and some carbonyl-type and cyclic monomers. We note that because of its lack of any substituent group, polyethylene cannot be polymerized anionically. We describe in a later section how to make living polymers that are similar to polyethylene by hydrogenation of polybutadiene.

Polybutadiene and its branched derivatives have been popular choices for basic studies because of their relatively low entanglement molecular weights and the usefulness of anionic polymerization for their synthesis. However, complications arise, because there are three ways in which the butadiene double bonds can be incorporated into the polymer molecule; cis, trans, and vinyl, and the actual chain structure depends on the catalyst and solvent used. The cis- and trans- forms are optical isomers arising from the rigidity of the double bonds in the backbone. A typical product might contain 45% cis, 48% trans, and 7% vinyl isomers. Because the entanglement molecular weight varies somewhat from one isomer to another, this leads to some inhomogeneity in the degree of entanglement. If the sample is hydrogenated to make a polymer similar to polyethylene, the optical isomerism is lost, but the vinyl groups remain. It is possible to reduce the vinyl content, but this leads to a broadening of the molecular weight distribution [20].

Copolymerization of two monomers, one to form a backbone and the other to form branches, can be used to make a remarkable range of materials. The backbone is first constructed, and the branch monomer is polymerized to form *macromonomers*, i.e., chains with a terminal double bond. Using this technique combs of various types can be made. If the backbone is very short and the grafting density is high, the result is a star. If the backbone is long and the grafting density is high, the resulting comb is called a "bottle brush."

Anionic polymerization produces linear polymers having the lowest polydispersity achievable by any process. By use of TGIC (Section 2.6.3.4) it has been shown that anionic polymerization can yield samples with polydispersity indexes well below 1.01 and MWD very close to the theoretical Poisson distribution. Anionic polymerization can also produce very high MW polymers having PDI values near unity. It is also the only living polymerization that works well with conjugated dienes like butadiene and isoprene, which are preferred for making model polymers because of their very low values of M_e. It is also the best way to make branched polymers. The truly living nature of the chain ends is advantageous during coupling reactions, and arms are much narrower in PDI, because they are grown by a truly living (termination free) process.

However, it was reported as early as 2002 [21] that carefully synthesized three-arm polystyrene stars can contain residual uncoupled arms, i.e., linear molecules. And more recently the use of TGIC analysis (described in Section 2.6.3.4) has revealed that even the most carefully carried out anionic polymerizations of branched structures produce some reaction byproducts that are larger or smaller than the target molecule. Perny et al. [22] discuss the problem of larger molecules, while Li et al. [23], Snijkers et al. [24], and Van Ruymbeke et al. [25] discuss the issue of fragments. In the latter case, the impurities relax faster than the molecule intended and act as a diluent for the latter, which should lead to acceleration of the relaxation of the target molecules. It has been suggested that this acceleration should not have a major effect if the purity is above 80%. We note, however, that at least one synthesis method designed to make H polymers yielded products that were revealed by TGIC to contain 50% or fewer H molecules, with the rest consisting of smaller, incompletely reacted species [23] However, using TGIC data to identify the byproducts and their concentrations it was still possible to use tube models to model their rheological behavior [26]. This subject is addressed in Chapter 9.

3.4.2 Living Free-Radical Polymerization (Reversible Deactivation Radical Polymerization—RDRP)

In recent years there has been rapidly growing interest in free-radical reaction schemes in which side reactions are suppressed, leading to *living/controlled* (i.e., nonterminated) free-radical polymerization techniques [27]. These processes are not truly "living," as there are always irreversible reactions occurring, but they can produce samples having low polydispersites.

Many variants of controlled/living radial polymerization techniques are in use. These include stable free-radical polymerization (SFRP) [28–38], nitroxide mediated polymerization (NMP) [29, 30], atom transfer radical polymerization (ATRP) [31] and degenerate transfer processes (DT), which include radical addition-fragmentation transfer (RAFT) [32] and catalyst chain transfer (CCT). These techniques have been used to polymerize many monomers, including styrene (both linear and star polymers) acrylates, dienes, acrylamides, methacrylates, and ethylene oxide. Research activity in this field is currently expanding rapidly, as is indicated by the many papers published and patents issued.

3.4.3 Model Polyethylenes for Research

Because of its low entanglement molecular weight and great industrial importance, it would be desirable to be able to synthesize polyethylenes having known structures using anionic polymerization. While this is not possible, polybutadiene (PBd) can be made by anionic polymerization and then hydrogenated to eliminate unsaturation [33] to produce a polymer that is very similar to polyethylene. However, Rochefort et al. [20] reported that it is not possible to synthesize polybutadiene having negligible vinyl content and also a very narrow molecular weight distribution. In addition, as mentioned above, double bonds can be incorporated into the polybutadiene molecule in three ways: cis, trans, and vinyl. While the cis-trans isomerism disappears after hydrogenation, the vinyl side groups produced by 1,2 addition, typically found in about seven percent of the monomer units, end up as ethyl branches after hydrogenation.

By use of chlorosilane chemistry, various branched structures can be prepared. For example, star-branched PBd can be prepared [20] and hydrogenated to produce analogs of star-branched polyethylene [34]. Hadjichristidis et al. [35] described the preparation of polyethylene analogs based on butadiene. Using the methods, they describe, a remarkable array of structures can be produced, including stars, H-shaped molecules, super-H molecules (three-armed stars at both ends of a backbone segment), pom-poms (multi-armed stars at the ends of a backbone) and combs of various types. Rheological data have been published for the polymers they described [36].

4 Linear Viscoelasticity— Fundamentals

The treatment of linear viscoelasticity presented in this chapter is sufficient for a full understanding of the models described in subsequent chapters. However, readers wishing to delve more deeply into this subject may wish to consult the monographs by Ferry [1] and Tschoegl [2]. Ferry treats the rheological properties of polymers, while Tschoegl's book is a compendium of empirical models and relationships between various linear material functions.

■ 4.1 Stress Relaxation and the Relaxation Modulus

4.1.1 The Boltzmann Superposition Principle

The *raison d'être* of this book is that rheological properties of the melt are very sensitive to the molecular structure of a polymer. Rheological properties describe how stress develops in a sample undergoing a prescribed deformation. They also describe the deformation that is caused by a prescribed stress. The most fundamental rheological experiment for a viscoelastic material is a step-strain test, and for melts this nearly always means a step *shear* strain. In a step shear-strain test, a sample is subjected to a sudden shear strain of magnitude, γ_0 at time $t = 0$. The shear stress is measured as a function of time, and the ratio of the stress to the applied strain defines the relaxation modulus, $G(t)$.

$$G(t) \equiv \sigma(t)/\gamma_0 \tag{4.1}$$

If the experiment is repeated, with the amount of strain doubled to $2\gamma_0$, another result will be obtained. If the resulting stress at any given value of t is exactly twice that measured in the first test at the same value of t, the relaxation modulus determined in the two experiments will be identical to each other. *From an experimental point of view this is a key feature of linear viscoelastic behavior*. The implication is
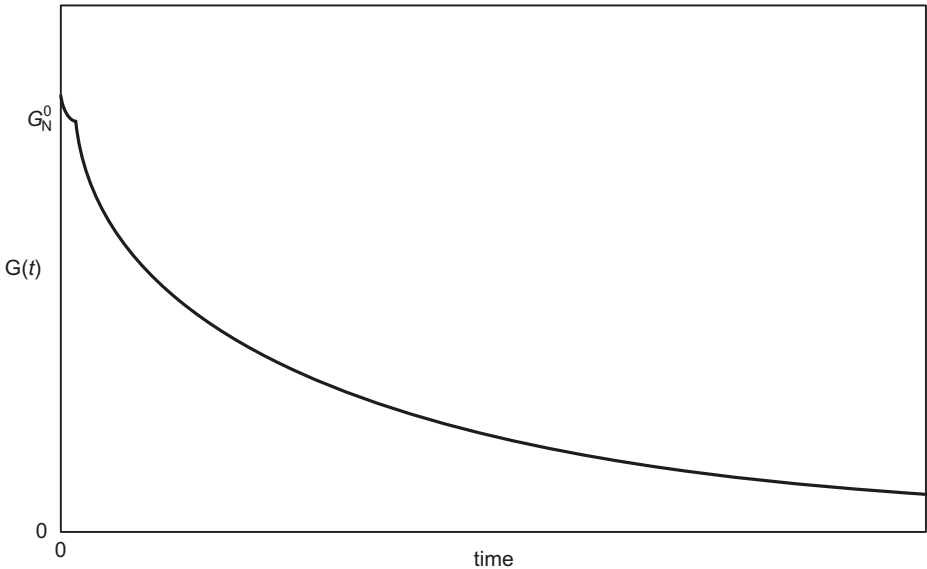
Figure 4.1 Typical stress relaxation curve for a molten polymer using linear scales for both axes. The pattern of the very fast relaxation at short times is not visible using a time scale that is suitable to show the final, long-term stage of the relaxation.

that in both experiments the strain is sufficiently small that the departure of the molecules from their equilibrium state is negligible. Thus, both experiments reveal the behavior of the polymer in its unstrained state. This, in turn, implies that the response to a series of small, step strains will be simply the sum of the responses to each step, where the same relaxation modulus governs each response.

Figure 4.1 shows a typical stress relaxation curve for a **highly entangled**, linear polymer sample in which all the molecules have the same molecular weight, i.e., a monodisperse sample. In this plot using linear scales, important phenomena that occur at very short times and at long times, where the stress is very small, cannot be seen. The same information is replotted in Fig. 4.2 using logarithmic scales for both axes. This has the effect of greatly expanding the behavior at very short times and very low stresses that were not visible using linear scales. The various features of this curve will be discussed in detail in Chapter 5. For the present, we will simply list the various zones in which distinctive relaxation mechanisms occur. At extremely short times there is a glassy zone in which the polymer is very stiff and has a very high "glassy modulus," G_g. This is followed by a "transition zone" in which additional mechanisms of relaxation come into play, and this leads into a *plateau zone*, in which very little relaxation occurs. Finally, at long times, a new mechanism of relaxation comes into play, and in this "terminal zone," the stress falls toward zero, which it must finally do in any liquid. The value of $G(t)$ in the zone of constant modulus is called the *plateau modulus*, and has the symbol G_N^0.
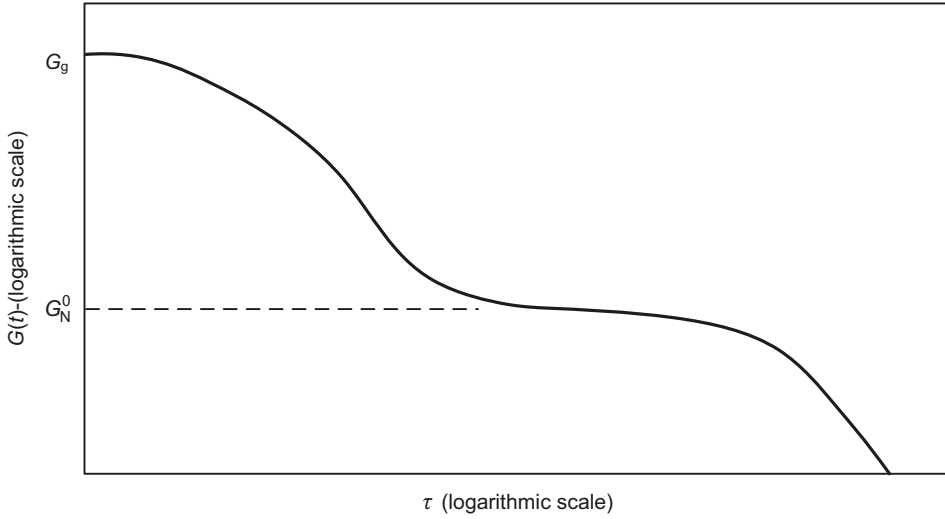
Figure 4.2 Stress relaxation curve for a linear, entangled, monodisperse polymer sample, where logarithmic scales are used for both axes. In this representation, distinct mechanisms of relaxation are apparent in the glassy, transition, plateau and terminal time zones.

Crosslinked elastomers do not flow, and the relaxation modulus of these materials drops to a non-zero constant value, the equilibrium modulus, G_e, which is its final plateau. It is important to note that if one is shown only the transition and plateau regions of the relaxation modulus curve for a monodisperse melt, this curve is virtually indistinguishable from that of a crosslinked material. Thus, in the plateau zone, a melt does an excellent impersonation of a rubber!

The additivity of responses can be expressed quantitatively by Eq. 4.2, which gives the stress as a function of time in response to a sequence of small shearing deformations, $\delta\gamma(t_i)$, occurring at times, t_i.

$$\sigma(t) = \sum_{i=1}^{N} G(t - t_i)\,\delta\gamma(t_i) \qquad t > t_N \tag{4.2}$$

Ludwig Boltzmann generalized this to give the response to a continuously varying shear deformation, rather than a series of step strains, by letting $\delta\gamma$ approach zero and writing Eq. 4.2 as an integral.

$$\sigma(t) = \int_{-\infty}^{t} G(t - t')\,\mathrm{d}\gamma(t') = \int_{-\infty}^{t} G(t - t')\,\dot{\gamma}(t')\,\mathrm{d}t' \tag{4.3}$$

Here, $\mathrm{d}\gamma(t')$ is the shear strain that occurs between t' and, $\mathrm{d}t'$, and $\dot{\gamma}$ is the shear rate during this period. Equation 4.3 is the form of the *Boltzmann superposition principle* for simple shearing deformations.

The Boltzmann superposition principle is valid for very small deformations, but it is also valid for very slow deformations, even if they are large. This is because polymeric liquids have a *fading memory* of past strains, which is reflected in the fact that $G(t)$ decays to zero at long times. As a result, as long as the accumulated strain is small for a time long enough for the memory to fade practically to zero, the response will still be governed by Eq. 4.3. However, it may prove impossible in practice to make a measurement at a sufficiently small shear rate for Eq. 4.3 to be valid, especially if very high molecular weight components or long chain branches are present. The stress generated may be too small to measure, the shear rate may be too small to be generated reliably, or the sample may degrade during the very long time required to reach steady state.

While we have considered only shearing deformations, the superposition principle applies to deformations having any kinematics. To generalize Eq. 4.3 to account for this, we need only replace the shear stress, shear strain, and shear rate by the corresponding tensorial quantities. The tensorial form of the Boltzmann superposition principle can then be used to determine all the components of the stress tensor arising from a deformation having any kinematics. Since we are interested here only in very small deformations, it is possible to use the infinitesimal strain tensor, whose components, $\gamma_{ij}(t,t')$ are related to the displacement vectors of neighboring particles of fluid particle at a time, t', relative to the "present" time, t, i.e., the time at which the stress is to be determined. The infinitesimal strain tensor and its use are described in detail by Dealy and Wang (ref. [3], p. 121). Using this tensor, we can write the general form of the Boltzmann superposition principle in terms of the components of the infinitesimal stress and rate-of-deformation tensors:

$$\sigma_{ij}(t) = \int_{-\infty}^{t} G(t-t')\,\dot{\gamma}_{ij}(t')\,dt' \tag{4.4}$$

For readers not familiar with this notation, a few words of explanation may be useful. The indices on a typical component of the stress tensor have the following meaning. The second index *j* indicates that this component of the stress acts in the x_j direction, while the first index indicates that it acts on a surface normal to the x_i axis. A component is positive when it acts on a fluid element in the plus x_j direction on the face of that element having the larger value of x_i. Thus, a tensile stress has a positive value, while a compressive stress is negative. Note that the opposite sign convention is used by some people, notably, R. B. Bird.

An important concept is that in an incompressible (constant density) fluid, an isotropic (i.e., the same in all directions) stress will cause no change in the shape or size of an element of the fluid. Since rheology deals with deformations, some isotropic portion of the total stress on an element is of no rheological significance. One way of recognizing this is to say that the stress tensor shown in Eq. 4.4 is the

extra or *viscous* stress, i.e., that portion of the total stress that will cause deformation in an incompressible fluid. We generally do not have any information about the isotropic component, and this means that there is uncertainty regarding the absolute value of normal stresses, i.e., those components for which $i = j$. However, this is not a problem, because in describing rheological behavior we will deal only with shear stresses and normal stress *differences*, for which isotropic components will cancel out.

While we will not need the general tensorial form of the superposition principle for the purposes of this book, we will show the result of its use to describe the special case of axisymmetric, uniaxial (tensile) extensional flow:

$$\sigma_{zz} - \sigma_{rr} = \int_{t'=-\infty}^{t'=t} 3\,G(t-t')\,d\varepsilon(t') = \int_{-\infty}^{t} 3\,G(t-t')\,\dot{\varepsilon}(t')\,dt' \qquad (4.5)$$

where σ_{zz} is the normal component of the stress tensor acting in the z (axial) direction, σ_{rr} is the normal component of the stress tensor acting in the r (radial) direction, $d\varepsilon(t')$ is the Hencky strain accumulating during the time interval dt', and $\dot{\varepsilon}(t')$ is the Hencky strain rate at time t'. The Hencky strain, $\varepsilon(t,t')$, that accumulates over the time interval from t' to t for a cylindrical sample of instantaneous length $L(t)$ is defined as:

$$\varepsilon(t,t') = \ln\left[L(t)/L(t')\right] \qquad (4.6)$$

The response to any deformation that is either very small, or occurs at very low strain rates, is given by Eq. 4.4. For example, the shear stress, $\sigma(t)$ following the sudden imposition at time t_0 of shearing at a steady rate, $\dot{\gamma}$, is given by:

$$\sigma(t) = \dot{\gamma}\int_{0}^{t} G(t-t')\,dt' \qquad (4.7)$$

The lower limit on the integral is zero rather than minus infinity, since the sample is known to be in a stress-free state at $t = 0$. The ratio of the stress to the shear rate is called the shear stress growth coefficient and has units of viscosity:

$$\eta^{+}(t) \equiv \sigma(t)/\dot{\gamma} = \int_{0}^{t} G(t-t')\,dt' = \int_{0}^{t} G(s)\,ds \qquad (4.8)$$

where $s \equiv (t-t')$. In the long-time limit, this transient function will approach the (steady-state) viscosity, which is thus given by:

$$\eta_0 = \lim_{t\to\infty} \eta^{+}(t) = \int_{0}^{\infty} G(s)\,ds \qquad (4.9)$$

Equation 5.4 leads to a formula for calculating the viscosity of a blend $\eta_{0,b}$. Since the M_w of a blend is simply the weighted average of those of its components, for a binary blend Eq. 5.4 implies that:

$$\eta_{0,b} = K\, M_w^\alpha = \left(w_1\, \eta_{0,1}^{1/\alpha} + w_2\, \eta_{0,2}^{1/\alpha}\right)^\alpha \tag{5.6}$$

where w_1 and w_2 are the weight fractions of the two components. This blending rule has been used as the basis for a method for inferring the molecular weight distribution from the curve of viscosity versus shear rate, as is mentioned in Chapter 8.

The effects of tacticity, comonomer, and long-chain branching on the zero-shear viscosity are discussed in later sections of this chapter.

■ 5.3 The Relaxation Modulus

5.3.1 General Features

Figure 5.2 shows the general shapes of the relaxation moduli for: A) an unentangled polymer; B) a monodisperse, entangled polymer; and C) a polydisperse polymer with M_w well above M_e. In addition, the relaxation modulus of a typical cross-linked elastomer is shown by curve D. At extremely short times, the only mechanism for relaxation is the stretching and bending of bonds, as there is no time for translational Brownian motion to act. This results in a very large "glassy" modulus, G_g, around 10^9 Pa. However, this parameter is not accessible using a standard melt rheometer, and a special instrument is required to achieve the very high-frequency deformations required. At longer, but still quite short times, short-range molecular motions come into play, and there is a transition zone in which there is a significant relaxation of stress. The behavior of all three types of sample is the same in this region, as entanglements do not interfere with this mechanism of stress relaxation. We will see in Chapter 6 that the longer-time portion of the transition zone can be described by a model developed by Rouse for dilute solutions and modified by Bueche for use with melts. If the molecular weight is below the critical value for entanglement (sample A) the stress continues to fall, entering a flow or terminal zone leading to the total relaxation of the stress.

However, for the entangled, monodisperse sample (B) there is a range of times during which further relaxation of any given molecule is almost completely blocked by the severe topological constraints imposed by the presence of other molecules. These topological constraints are universally referred to as "entanglements." During this period, further relaxation is strongly supressed, and there is a plateau in the curve. The value of the relaxation modulus corresponding to this plateau is
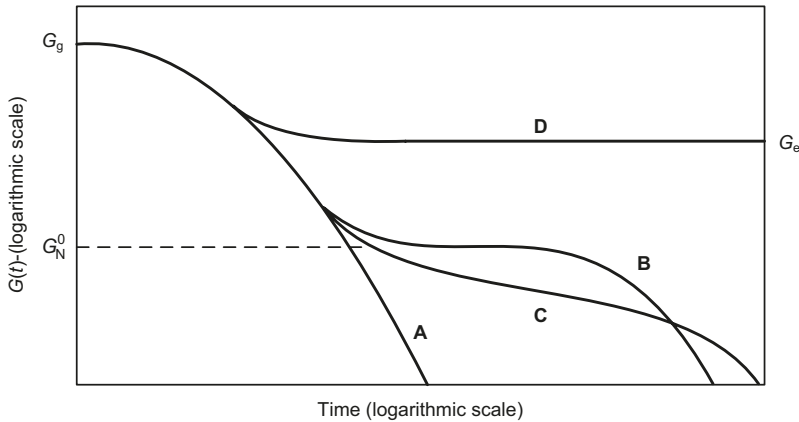
Figure 5.2 Relaxation moduli of three samples of a linear polymer: A) an unentangled molten sample, B) an entangled, monodisperse molten sample, C) an entangled, polydisperse molten sample, and D) a cross-linked sample. At short times, all the samples relax first by a glassy mechanism and then by Rouse relaxation involving only very short segments of the chain (log scales). The unentangled melt then flows in the terminal zone. The entangled, monodisperse melt has a plateau modulus followed by terminal relaxation, while for the polydisperse melt the plateau zone of the longest molecules overlaps with the terminal zones of the shorter molecules.

the *plateau modulus* G_N^0. Values of this parameter for several polymers are listed in Appendix A. Establishing a reliable value for G_N^0 is not as straightforward as it might first appear to be and several methods for estimating G_N^0 from experimental data are described in Section 5.7. Eventually, a molecule escapes its entanglement constraints by means of the relatively slow process of wriggling along its length. In the "tube model" (Doi-Edwards model) for relaxation presented in Chapter 6, this wriggling motion is called *reptation*. This leads finally to the terminal zone, in which complete relaxation becomes possible.

Finally, sample (C) shows the relaxation modulus for a polydisperse material having a polydispersity index (M_w/M_n) of about four, with $M \gg M_e$ The broadening of the molecular weight distribution results in the loss of a true plateau, because there is now a broad range of times over which relaxation occurs via the slow process of escape from entanglements

It is important to note that short-time relaxation mechanisms arise from molecular phenomena that are localized along the molecule. They depend only on the local structure of the chain and not its large-scale architecture. They thus provide no information regarding molecular weight, molecular weight distribution or branching. Since our primary concern in this book is how structure affects rheological behavior, we will mainly be interested in the plateau and terminal zones. If the sample of interest were made up of long, linear molecules all having the same molecular

weight, there would be a distinct plateau, and we could easily disregard data in the transition zone. However, we would like to relate rheological behavior to the structure of polydisperse systems, and schemes for dealing with this problem are discussed in several sections of this book.

5.3.2 How Can a Melt Act like a Rubber?

It is of interest to compare the behavior of the monodisperse polymer with $M \gg M_e$ (curve B) with that of the cross-linked elastomer, (rubber) which is illustrated by curve D. At very short times the rubber also shows glassy behavior, and at somewhat longer times, it is able to relax by means of Brownian motion involving short segments of chains. However, it cannot flow because of chemical cross-links, and the relaxation modulus falls only to an *equilibrium modulus*, G_e, at long times. Thus, at times up to the end of the plateau zone, the relaxation modulus of the highly entangled melt is indistinguishable from that of the rubber. This is the reason why a melt can impersonate a rubber in short-time phenomena. For example, "silly-putty" or "bouncing putty" is poly(dimethyl siloxane), which is molten at room temperature. It can be easily shaped by hand, and if left on a table-top, it will flow very slowly into a puddle like any other liquid. However, if rolled into the shape of a ball and dropped on a table, it bounces quite nicely, undergoing no change of shape in the process! This is because the time during which the ball is in contact with the table is much shorter than the time required to reach the end of the plateau zone, and the melt acts exactly like a cross-linked rubber.

The similarity between the behavior of an entangled melt and that of a rubber led to the definition of the *molecular weight between entanglements* M_e, in terms of the plateau modulus G_N^0 by analogy with the equilibrium modulus of a cured elastomer. This important polymer property, M_e, is discussed in detail in Section 5.8.

■ 5.4 The Storage and Loss Moduli

Small-amplitude oscillatory shear is usually used to determine the linear viscoelastic characteristics of molten polymers. Figure 5.3 shows the storage moduli of the samples whose relaxation moduli are shown in Fig. 5.2. Note that logarithmic scales are used for both axes. The same features are present as in a plot of $G(t)$, but the terminal zone is now found at the left end of the curve, while the short-time response corresponds to high-frequency behavior. And here again it is the behavior in the plateau and terminal zones that is sensitive to molecular structure and is thus of primary interest to us.
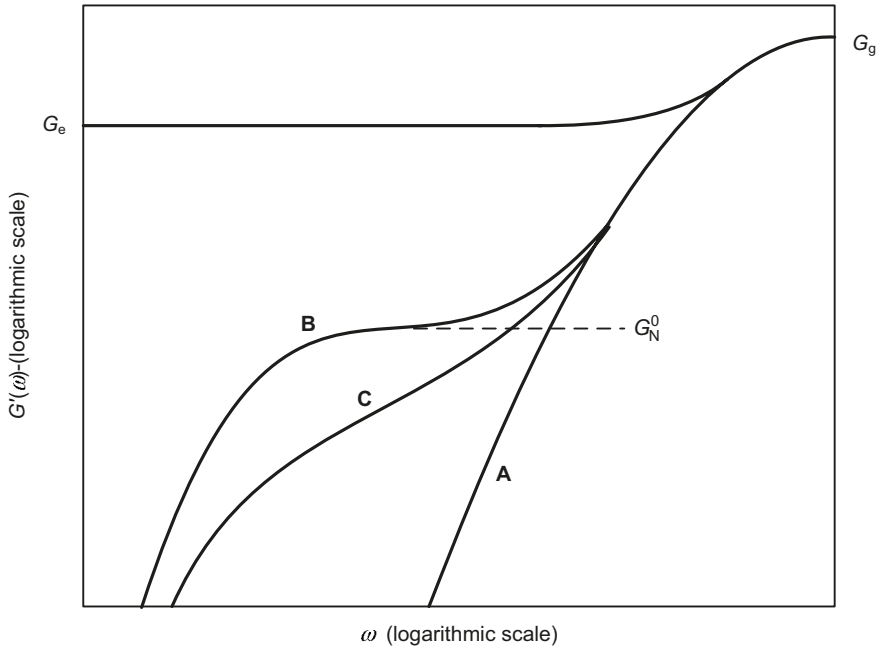
Figure 5.3 Storage moduli of same materials as in Fig. 5.2: A) unentangled polymer, B) entangled, monodisperse melt, C) entangled, polydisperse melt, D) cross-linked polymer (logarithmic scales). The plateau modulus is G_N^0, G_g is the glassy modulus, and G_e is the equilibrium modulus of the cross-linked material.

Figure 5.4 shows storage and loss modulus mastercurves of Plazek [18] for a poly(vinyl acetate)]. This sample was not perfectly monodisperse, and while the plateau zone can be identified, there is no region in which the storage modulus is truly flat. Relaxation times governing the various relaxation times involved did not have the same temperature dependency, but Plazek achieved reasonable superposition using only two time-shift factors, one for short-time behavior and another for the plateau and terminal zones. There is a minimum in the loss modulus in the plateau zone, reflecting the fact that there is a marked decrease of energy dissipation in this region.

At low-frequencies the slopes on these log-log plots become one for (G'') and two for (G'). We can understand this limiting behavior at very low frequencies by reference to Eqs. 4.40a and 4.40b. The denominators approach unity, and if the longest relaxation time τ_1 is significantly larger than τ_2 the numerator will be dominated at long times by τ_1, which is called the *terminal relaxation time*. We will see in Chapter 6 that some molecular models predict a discrete spectrum for monodisperse systems in which the longest relaxation time is significantly larger than the next longest one. Thus, in the terminal zone the storage modulus becomes proportional to the square of the frequency, while the loss modulus becomes proportional to the frequency.

as MWD and LCB content (though such work is still in its infancy). In Chapter 11, the reader will be appraised of recent progress on these fronts in the development of theories of the nonlinear viscoelastic behavior of polymers. Our principal concern is the relationship between rheological behavior and molecular structure in highly entangled polymers. Thus, the fast, localized molecular motions that dominate the behavior of unentangled systems, such as very dilute solutions and low molecular weight melts, are not of primary interest to us. However, the Brownian motion that every element of a molecule is constantly undergoing is ultimately the cause of all molecular motion in the absence of flow, and some key parameters that arise in the modeling of the dynamics of unentangled polymers will be found to carry through into models of entangled ones. Thus, we begin our treatment of polymer dynamics with a summary of a theory for unentangled polymers.

■ 6.2 The Rouse-Bueche Model for Unentangled Polymers

6.2.1 Introduction

If one attempts to model the dynamics of a single long polymer molecule in a very dilute solution starting from an atomically detailed picture of the molecule, the task rapidly becomes impossibly complicated because of the number of bonds that must be taken into account and the limitations on the motion of the backbone bonds with respect to each other. Fortunately, it is possible to achieve a drastic simplification of the problem if we are not interested in the very short-range motions that are responsible for the initial, very fast stages of relaxation after the imposition of a deformation on the system. In modeling the slower dynamics of a polymer molecule in a dilute solution, many useful results have been derived by use of a model in which the molecule consists of a number of *submolecules,* each containing enough backbone bonds that it behaves like a freely-jointed, Gaussian chain. We saw in Chapter 2 that about ten backbone bonds are required to form a unit that acts like the single link in a freely-jointed chain, so a submolecule must contain many such units.

How many monomer units are required to form a submolecule? It is not necessary to select a specific number of monomer units, but it must be large enough so that there are enough degrees of freedom within the submolecule so that it behaves like a Gaussian chain. It is possible to calculate the minimum length of a submolecule that would allow it be represented by a freely-jointed chain, and for typical, flexible synthetic polymers this corresponds to about 100 chemical bonds or 100 backbone atoms. On the other hand, a description of the whole molecule sufficiently detailed

for our purposes requires that it contain many submolecules, and hence the size of the submolecule cannot approach that of the entire macromolecule. It follows that this coarse-grained model of a polymer molecule involving submolecules is only appropriate for long molecules containing at least many hundreds of bonds.

The freely-jointed chain picture is used in the next section as the basis for a model for the viscoelastic behavior of a dilute solution. It is important to keep in mind, however, that we cannot expect the model to describe the very short-time behavior involving short-range interactions between segments of the molecule that are within a submolecule, as these are not accounted for in this coarse-grained picture.

6.2.2 The Rouse Model for the Viscoelasticity of a Dilute Polymer Solution

In the Rouse model of the dynamics of a polymer molecule in a dilute solution [4], the mass of a submolecule is assumed to be concentrated in a bead at its center, and the N beads making up the model chain are attached to each other by N-1 springs. The elasticity of the submolecule, and thus of the molecule, is an entropic effect that arises from Brownian motion, and thermodynamic arguments show that for small or modest molecular extensions, the spring force should be proportional to kT times the extension, where k is Boltzmann's constant. In the Rouse model, the molecule can be stretched indefinitely, and this reminds us that the Gaussian chain model is only valid when the total extension of the molecule is not too large, i.e., when R (the root-mean-square end-to-end distance) is less than about 0.3 nl, where n is the number of backbone bonds, and l is the length of a single backbone bond.

In the Rouse model, the drag force exerted on a bead as it moves through the solvent is assumed to be given by Stokes' equation for the drag on a rigid sphere moving through a Newtonian fluid. This drag force is modeled in terms of a monomeric friction coefficient, ζ_0, which is the drag force per monomer unit divided by the velocity of the solvent relative to that of the monomer unit and has SI units of kg/s. The subscript zero on the friction coefficient indicates that it applies to a dilute solution in its theta state, i.e., that there are interactions between the polymer and the solvent that cancel out the interactions between the polymer and itself, so that the conformation of the polymer molecule is a random flight, unaffected by these interactions. We note that the definition of ζ_0 used by Berry and Fox in their widely cited article [5] is different from the one used here but is proportional to it.

Relaxation after deformation results from the restoring *entropic-spring* force acting against the viscous resistance of the solvent (indeed, all results in this and subsequent sections assume spring forces are entropic in origin; in practice, there may by enthalpic contributions to spring forces). So, the characteristic time of the relaxation is thus proportional to ζ_0 and inversely proportional to kT.

Because of the many degrees of freedom in the chain, the relaxation process is actually governed by a series of relaxation times. In the Rouse model, there is one relaxation mode, with relaxation time τ_p, for each value of the index p up to N, the number of submolecules in the chain, as shown by Eq. 6.1:

$$G(t) = \frac{\rho\,R\,T}{M} \sum_{p=1}^{N} e^{-2\,t/\tau_p} = \frac{\rho\,R\,T}{M} \sum_{p=1}^{N} e^{-t/\tilde{\tau}_p} \tag{6.1}$$

The reason for the factor of two appearing in the exponential in Eq. 6.1 is that there is a potentially confusing factor of two difference between two relaxation times that might be defined within the Rouse model. The relaxation time for the *stress* contribution of the pth mode (which we here denote as $\tilde{\tau}_p$) is exactly half the relaxation time of *molecular orientation* from the pth mode (which we here denote as τ_p). That is, $\tau_p = 2\,\tilde{\tau}_p$. The mathematical reason for this factor of two is that stress depends essentially on the square of the orientation of chain subsegments. In the following, we take care to distinguish these two definitions of relaxation time.

We recall that the number of submolecules N is arbitrary within limits, so if terms for which p approaches N made a significant contribution to the sum, the Rouse model would not be valid, as this would imply that phenomena occurring *within* a submolecule (which are not accounted for in the model) are affecting the stress. It is thus required that the series converge for p somewhat less than N. If the series converges for $p < N/5$, the relaxation times τ_p and $\tilde{\tau}_p$ can be accurately approximated by:

$$\tau_p = \frac{b^2\,N^2\,\zeta_0}{3\,\pi^2\,p^2\,k\,T}; \qquad \tilde{\tau}_p = \frac{b^2\,N^2\,\zeta_0}{6\,\pi^2\,p^2\,k\,T} \qquad p = 1, 2, 3, \ldots \tag{6.2}$$

where b is the statistical segment length defined in Eq. 2.11 as $\left(\langle R^2 \rangle_0 / N\right)^{1/2}$, and N is the degree of polymerization, i.e., the number of monomer units per molecule, M/M_0. (Ferry [6] uses the symbol a for this length.) These *Rouse relaxation times* play a central role in all the relaxation models discussed in this book, as they govern the time scales for the basic molecular motions that are involved, directly or indirectly, in all relaxation processes.

The Rouse modes of molecular motion are to some degree analogous to the modes of vibration of a string fastened at both ends, as shown in Fig. 6.1. The frequency of vibration is proportional to n/l, where here n is the number of the mode and l is the length of the string. And the wavelength is $2\,l/n$. Mode one corresponds to a wavelength of $2\,l$, and this is indicated by the top curve. Mode two corresponds to a wavelength of l, and this is indicated by the second curve. Mode three has a wavelength of $2\,l/3$, and this is shown by the third curve. Note that as the frequency increases, higher and higher modes are activated, and the corresponding motion of the string involves the coordinated motion of shorter and shorter segments of the string.
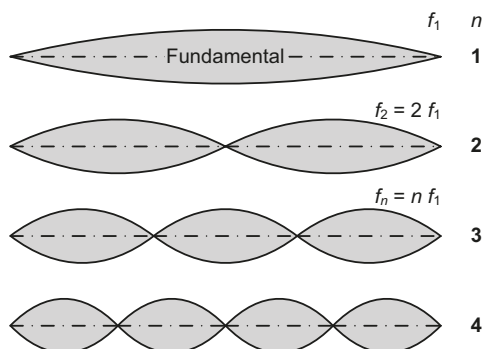
Figure 6.1 Modes of motion in a vibrating string, which are analogous to the modes of motion in a polymer molecule according to the model of Rouse. Modes 1 through 4 are shown. Higher modes involve the coordinated motion of successively shorter segments of the string, as higher Rouse modes represent the coordinated motions of successively smaller groups of submolecules. The analogy is far from perfect, as a molecule is not fixed at its ends

The longest Rouse time, corresponding to $p = 1$, is especially important and is called the *longest Rouse relaxation time.* As with the individual Rouse modes, the longest relaxation time for the stress, and the longest relaxation time for the molecular orientation, are separated by a confusing factor of two (see the previous discussion following Eq. 6.1). Unfortunately, this has led to discrepancies in the literature as to which of the two times should be called "the Rouse time," with rheologists tending to favor the stress relaxation time, while theoretical physicists often favor the reorientation time. In this book, we shall refer to the two timescales as the *Rouse reorientation time* (giving this the symbol τ_r) and the *Rouse stress relaxation time* (giving this the symbol τ_R). While for dilute polymers and unentangled melts the Rouse stress relaxation time τ_R is the most relevant, when we come to discuss entangled melts we will find the Rouse reorientation time τ_r is the more useful quantity, as it sets the timescale for primitive path fluctuations (Section 6.4.2) and stretch relaxation (Sections 11.2.1 and 11.3.2). The two times are given as:

$$\tau_r = \frac{b^2 \, N^2 \, \zeta_0}{3 \, \pi^2 \, k \, T}; \qquad \tau_R = \frac{b^2 \, N^2 \, \zeta_0}{6 \, \pi^2 \, k \, T} \tag{6.3}$$

Note that since $N = M/M_0$, both τ_r and τ_R are proportional to M^2 for a given polymer.

Rouse assumed the molecule to be *freely draining,* i.e., that the effect of the flow of solvent past one part of the molecule has no effect on another part. Another way of saying this is that he assumed no *hydrodynamic interaction.* As is noted in Section 2.5.3 on intrinsic viscosity, this led to predictions that were not in accord with observations for dilute polymer solutions. Zimm later developed a model that took into account hydrodynamic interaction, but it is not necessary to consider this here, as it is not relevant to our discussion of melt behavior where there is no solvent.

■ 7.2 Limitations of Double Reptation Theory

Let us start by illustrating the conceptual limitations of the double reptation idea. Consider the case of a polymer of high molecular weight at a volume concentration ϕ_L in a matrix of a polymer of much lower molecular weight. This case was considered in Section 6.4.4.2, and we found that the double reptation model predicts two relaxation peaks in G'', a peak at a high frequency roughly equal to the inverse of the reptation time, $\tau_{d,S}$, of the short chains, and a low-frequency peak, whose frequency is the inverse of half the reptation time, $\tau_{d,L}/2$, of the long chains. The height of the low-frequency peak is predicted by double reptation to be proportional to the square of the volume fraction of long chains ϕ_L^2. These predictions were found to be in good agreement with data for some binary blends of polybutadiene. For those data, the concentration of long chains was high enough that each long chain was entangled with other long chains.

Figure 7.1 Illustration of a long polymer (artificially straightened for illustrative purposes) entangled with much shorter chains, where the long-chain concentration is too low to permit entanglements between long chains

Let us now consider a more severe test of double reptation in which the long chains are dilute, meaning that entanglements of the long chains with other long chains are negligible; see Fig. 7.1. This is the case if the product of the concentration ϕ_L of the long chains and their molecular weight M_L is less than the entanglement threshold for the melt; i.e., $\phi_L M_L < M_C$). Figure 7.2 shows experimental $G'(\omega)$ data for this case. The volume fraction of long chain in this binary blend of monodisperse polystyrenes is only $\phi_L = 0.015$, and its molecular weight is held fixed at $M_L = M_2 = 1,810,000$, while the molecular weight of the short matrix chains is varied from $M_S = M_1 = 71,400$ to $775,000$ [1]. Notice from Fig. 7.2 that, as expected, there is a fast relaxation mode at high frequency with a high plateau modulus. The frequency at which $G'(\omega)$ begins to decrease from this plateau decreases with increasing molecular weight of the short chain. Thus, the relaxation time associated with the "fast" relaxation mode clearly increases with increasing molecular weight of the short chain. This much is expected from double reptation theory.

There is also a second relaxation mode that is revealed by the "shoulder" in the data at low frequency. This second mode, which is generated by the relaxation of the
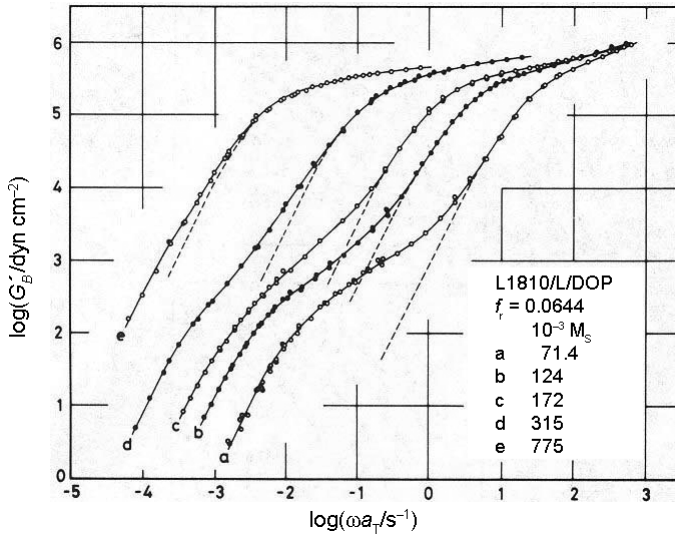
Figure 7.2 Storage modulus of 60 vol% solutions of bidisperse polystyrene in dioctylphthalate. The molecular weights M_L is 1,810,000 and M_S values are shown. The volume fraction ϕ_L of long chain is 0.015, which is low enough to be unentangled with itself. The dashed lines are G' of monodisperse, low molecular weight polystyrenes at 60% concentration; adapted from Watanabe [1]

long chains, is expected to be present, according to double reptation theory, but in double reptation theory it would appear as a relatively flat plateau, rather than as a more gradual "shoulder". In addition, the relaxation time associated with this mode would in double reptation theory be independent of the molecular weight of the short chains, since it is caused by reptation of the long chains. However, in Fig. 7.2, the long chain molecular weight is held fixed, yet the "shoulder" clearly shifts its location with the molecular weight of the short chains. Thus the relaxation time of the slow mode depends on the molecular weight of the short chain, in contradiction to double reptation theory. Clearly, double reptation theory cannot apply to this case. Double reptation also predicts that the magnitude of the slow relaxation mode should be proportional to ϕ_L^2, while these experiments instead show proportionality to ϕ_L [2].

The dashed lines in Fig. 7.2 are the $G'(\omega)$ curves for the pure short chains. If these dashed curves are subtracted from the data for the binary blends in Fig. 7.2, the contribution from the long chains is obtained, and this is plotted in normalized form in Fig. 7.3 for several different dilute blends of long chains in short chains [3]. These long-chain contributions to $G'(\omega)$ are proportional to ϕ_L, not ϕ_L^2, and the relaxation of the long chain clearly is described by multiple relaxation modes, not a single mode, which would produce a flat plateau. Both of these findings disagree with predictions of double reptation theory. Notice, however, that the shapes of the curves for the long-chain contribution to $G'(\omega)$ in Fig. 7.3 are similar to those of

the curves predicted by the Rouse theory in Fig. 6.3. Thus, when the long chains are dilute, the long-chain contribution to the linear viscoelasticity is similar to that predicted by the Rouse theory, which was obtained by neglecting entanglements (see Section 6.2). While the solution considered in Figs. 7.2 and 7.3 has entanglements of long chains with short chains, it lacks significant entanglements of long chains with other long chains, and it is the lack of such long-chain/long-chain entanglements that produces the Rouse-like response observed in Fig. 7.3. Thus, when the long chains are dilute, double reptation theory fails, but a version of the Rouse theory, describing "constraint-release Rouse" relaxation, becomes applicable.
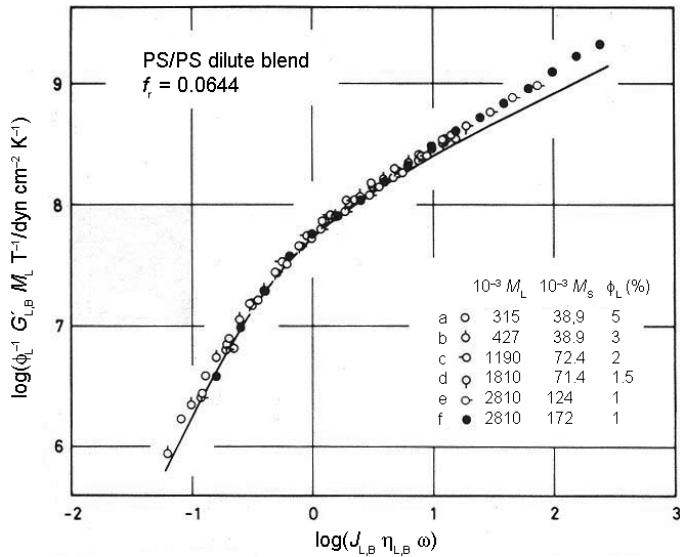
Figure 7.3 Dependence of the normalized storage modulus $M_L G'_{L,B}/c_L R T$ on reduced frequency $\omega \langle \tau_{L,G} \rangle = \omega J_{L,B} \eta_{L,B}$ for dilute blends of high-molecular weight polystyrene at volume fraction ϕ_L in a matrix of much shorter polystyrene chains, or of dilute polyisoprene in polybutadiene. Here, G'_B is the contribution of the long chain to the storage modulus, i.e., the storage modulus of the dilute blend with the matrix contribution subtracted off, and ϕ_L is the concentration of the long chain in units of mass/volume. R is the gas constant. $\langle \tau_{L,G} \rangle$ is an average relaxation time defined in Watanabe [2]. The molecular weights M_L and M_S of the long and short chains are given in the figure. The dashed line is the prediction of Rouse theory. Adapted from Watanabe et al. [1]

■ 8.4 Methods Based on Double Reptation

In Chapter 6, the *double reptation* modification of the Doi-Edwards model for polydisperse systems was introduced in Chapter 6, and we repeat the basic idea here as Eq. 8.1.

$$\frac{G(t)}{G_N^0} = \left\{ \int_{M_e}^{\infty} w(M) \left[F(t,M) \right]^{1/2} \, dM \right\}^2 \tag{8.1}$$

This was introduced as a simple method to account for constraint release, and in its original form it does not account for contour length relaxation, so that it predicts that the zero-shear viscosity is proportional to M^3 rather than to $M^{3.4}$. As an empirical correction to the model, Mead [23] suggested simply making the relaxation time in the relaxation function proportional to $M^{3.4}$ instead of M^3. Of course this does not constitute a full modeling of contour length fluctuations, but it does guarantee the correct dependence of η_0 on M as calculated from $F(t,M)$. For a single exponential relaxation function with the relaxation time equal to $K\,M^{3.4}$:

$$F(t,M) = \exp\left(\frac{-t}{K\,M^{3.4}} \right) \tag{8.2}$$

If Eq. 8.1 were a good model for polydisperse systems, and if the integral could be inverted, the molecular weight could be determined once $G(t)$ had been measured. But to accomplish this, several issues must be addressed.

1. The relaxation modulus must be fitted by an equation.

2. The relaxation function for monodisperse polymer $F(M,t)$ must be specified.

3. Since the model only applies to the plateau and the terminal relaxations, other mechanisms, particularly the high frequency (short-time) Rouse modes, will pollute the curve of $G(t)$ and interfere with the MWD determination, as these do not depend on the molecular weight.

However, the properties most often used to characterize linear viscoelastic behavior are the storage and loss moduli rather than the relaxation modulus. In Section 4.4 we described several techniques for inferring continuous or discrete relaxation spectra from such data. However it is important to note that in the transformation to a discrete spectrum, some information is always lost, and this can affect the reliability of subsequent calculations.

As for the form of the monodisperse relaxation function, several models have been proposed. First, since double reptation is a direct descendent of the Doi-Edwards reptation model, it seems appropriate to use the original D-E modulus, which is given by Eq. 8.3.

$$F(t,M) = \frac{8}{\pi^2} \sum_{n=1\,(\text{odd})}^{\infty} \frac{e^{-t\,n^2/\tau_0(M)}}{n^2} \tag{8.3}$$

Noting that this series is dominated by the first term and that in a polydisperse system, the details of the spectrum will be smeared out to some degree, Tsenoglu [24] suggested the use of a single exponential (Eq. 8.4).

$$F(t,M) = e^{-t/\tau_0(M)} \tag{8.4}$$

And there is an even simpler possibility. Mead (see ref. [23], App. A) points out that Tuminello's method, which is based on the curve of $\left[G'(\omega)/G_N^0 \right]^{0.5}$ versus frequency, can be considered to be a special case of double reptation in which the relaxation function is a step function (Eq. 8.5).

$$\begin{aligned} F(t,M) &= 1 \qquad t < \tau_0 \\ F(t,M) &= 0 \qquad t > \tau_0 \end{aligned} \tag{8.5}$$

A two-parameter empirical equation (the BSW function) was proposed by Baumgaertel et al. [25], and des Cloizeaux [26] developed a more complex form from a theory. The most popular choice, however, has turned out to be the single exponential, as it is simple but often adequate. Wasserman and Graessley [27] made a critical comparison of the four forms of $F(t,M)$ mentioned above.

The problem remains of inverting the integral, and it is the most difficult one. Equation 8.1 is of a form that arises often in applied physics and is called a Fredholm integral equation of the first kind. It is an example of an "ill-posed" problem, which means, in this case, that noise or incompleteness in data generally result in a system that has no unique solution for $w(M)$. The same type of problem arises in the inference of a relaxation spectrum from data for the storage and loss moduli as was explained in Section 4.4.

Mead [23] noted that to overcome the ill-posedness it is necessary to provide additional information and to use specialized numerical methods. In the case of the step function choice for $F(t,M)$ he was able to find an analytical solution to the inversion problem, while for other choices, he recommended the use of the CONTIN software, originally designed for use in treating light scattering data [28]. This makes use of a non-linear regularization parameter that is adjusted in accord with the noise level in the data.

In order to guide the problem to the correct solution, several normalization conditions are imposed, for example that the weight fractions sum to one.

$$\int_0^{\infty} w(M)\,\mathrm{d}M = 1 \tag{8.6}$$

Comparing the MWD determined using this technique to GPC results for several systems, the agreement was quite good for higher molecular weight species, but the amount of low molecular weight material present was overestimated. In general, Mead found that the broader the MWD, the harder it is to resolve low molecular weight material using rheology. In general, a broad MWD will cause his method to indicate too low a value of M_w, because the low molecular weight species "dilute" the larger molecules, an effect that is not accounted for in the model. Also the model predicts that the MWD has a significant effect on η_0, but as noted in Section 5.2.2 this is counter to most observations.

Wasserman [29] also developed a method for calculating MWD that is based on the double reptation model. However, whereas Mead [23] chose to use the integral form of the equation and employed various mathematical transforms to manipulate it, Wasserman used discrete variables and numerical techniques. Thus, he writes the double reptation relationship as:

$$G(t) = G_N^0 \left[\sum_{i=1}^{c} w_i \sqrt{F(t, M_i)} \right]^2 \tag{8.7}$$

He chose to use the BSW empirical relaxation function [25], which was implemented in the manner described by Wasserman and Graessley [27]. Each datum (G_k, t_k) thus yields an algebraic equation in which all the $F(M_i, t_k)$ coefficients are known, and the system of such equations can, in principle, be solved by linear regression for the variables (w_i). Wasserman [29] discusses the problems that arise in this procedure. He notes that since experimental data are available only over a limited range of frequencies, MWD can only be determined within certain limits, and he provides equations for estimating the molecular weight limits.

But the problem is still ill-posed, and Wasserman [29] used Tikhonov-Mallows regularization to obtain a solution. He used the same technique to infer a discrete spectrum $\{G_k, t_k\}$ from experimental data in the form of $\{G_k^*, \omega_k\}$. Wasserman [31] points out that the selection of the regularization parameter, λ_R, is subjective and depends on whether one wants a smooth solution, with a high degree of certainty in the calculated weight functions (large λ_R), or less certainty and a theoretically more accurate distribution (small λ_R). If λ_R is too high, the solution indicates too much high MW material, but if it is too small, artificial maxima and minima appear in the MWD. The problem of selecting the best value for λ_R was addressed by Honerkamp and Weese [30], who compared several methods and concluded by recommending the "self-consistent" method, in which the value is set in accord with the noise level in the data. Weese [31] developed a "Fast Tikhonov Regularization (FTIKREG)" algorithm based on this method. This tool has been used to determine MWD, for example by Léonardi et al. [32], who discuss the method in more detail.

Nobile and Cocchini [33] used the double reptation model to calculate the relaxation modulus, the zero-shear viscosity and the steady-state compliance for a given MWD. They compared three forms of the relaxation function for monodisperse systems: the step function, the single integral, and the BSW. In the BSW model, they set the parameter β equal to 0.5, which gives $J_s^0\, G_N^0$ equal to 1.8. The molecular weight data were fitted to a Gex function to facilitate the calculations (see Section 2.2.4 for a description of distribution functions). For the step function form of $F(M,t)$, the relaxation function is given by Eq. 8.8.

$$G(t) = G_N^0\ \Gamma^2\left[\left(\frac{a+1}{b}\right),\left(\frac{t}{\tau}\right)^{b/\alpha}\right] \Bigg/ \Gamma^2\left(\frac{a+1}{b}\right) \tag{8.8}$$

where: $\tau = K\, M_0^\alpha$, $K = \eta_0 / M^\alpha$, a, b, and c are parameters of the Gex distribution, and $\Gamma(x)$ is the gamma function.

Using the analytical result (Eq. 8.8), they found that for mildly polydisperse systems, the zero-shear viscosity depended only on the weight average molecular weight as has often been reported, but that for broader distributions, the zero-shear viscosity varied with the polydispersity. They reported an approximate form of this dependency, valid when $M_w/M_n > 1.5$, which is shown here as Eq. 8.9.

$$\eta_0 = k\left(\frac{M_z}{M_w}\right)^{0.8} M_w^{3.4} \tag{8.9}$$

Nobile and Cocchini [34] then used the step relaxation function in the double reptation integral, together with the Gex molecular weight distribution, to calculate the parameters of the latter for several polymers. In order to obtain $G(t)$ from dynamic data, they approximated the former by a series of linear segments. Comparing their results with GPC distributions they found that their predicted values of M_z/M_w were fairly accurate but that the values of M_w/M_n were not. It must be recalled here that in order to arrive at an analytical form for the relationship between $G(t)$ and MWD, a number of simplifying assumptions must be made. These include neglecting Rouse modes, tube length fluctuations, and "dynamic dilution." In addition, the step relaxation function and the Gex molecular weight distribution were assumed. Cocchini and Nobile [35] later improved their method by using the relaxation function proposed by Thimm et al. [36] and accounting for the contribution of Rouse modes.

Another method that makes use of the double reptation model and the assumption of a Gex MWD is that of Guzmán et al. [37]. They also account for the effect of unentangled chains. Their method avoids the use of a regularization technique to infer $G(t)$ from dynamic data, and their analysis provides an estimate of the reliability of the results.

10 Nonlinear Viscoelasticity

■ 10.1 Introduction

In Chapter 4, it was noted that linear viscoelastic behavior is observed only in deformations that are very small or very slow. The response of a polymer to large, rapid deformations is nonlinear, which means that the stress depends on the magnitude, rate and kinematics of the deformation. The Boltzmann superposition principle is no longer valid, and nonlinear viscoelastic behavior cannot be predicted from linear properties. There exists no general model, i.e., no universal *constitutive equation* or *rheological equation of state* that describes all nonlinear behavior. The constitutive equations that have been developed are of two basic types; empirical continuum models, and those based on a molecular theory. We will briefly describe several examples of each type in this chapter, but since our primary objective is to relate rheological behavior to molecular structure, we will be most interested in models based on molecular phenomena. The most successful molecular models to date are those based on the concept of a molecule in a tube or of slip links, which were introduced in Chapter 6. We therefore begin this chapter with a brief exposition of how nonlinear phenomena are represented in tube models. A much more complete discussion of these models is provided in Chapter 11.

■ 10.2 Nonlinear Phenomena—A Tube Model Interpretation

As was explained in Chapter 6, tube models are based on a picture in which the constraints imposed on a highly entangled polymer molecule (*test chain*) by the surrounding ones are modeled as a *tube* having a characteristic length and diameter [1]. This is an example of a mean-field theory, in which the effects of surrounding molecules on the test chain are averaged together, drastically reducing the computational effort that is required to make rheological predictions compared to that required

for a detailed molecular dynamics model. Tube models have shown promise in the prediction of linear viscoelastic behavior and some types of nonlinear behavior for certain types of molecular structure.

In response to a sudden deformation, the tube is deformed, i.e., the distribution of orientations of the chain segments is shifted from its equilibrium distribution, and the relaxation of a molecule back to its undeformed configuration is constrained by its confinement in the tube. When the imposed deformation is very small, the first relaxation process that occurs is equilibration within the tube, as mentioned briefly in Section 6.3.5. Equilibration involves the redistribution of stress along the chain within the tube. Further relaxation can only occur as a result of the molecule escaping the constraints of the tube, and this requires it to slither along or *reptate* out of its tube. This is a much slower process and is the reason that there is a plateau in the relaxation modulus for entangled polymers with a very narrow molecular weight distribution. This shows up in the linear relaxation spectrum $H(\tau)$ in the form of two peaks, one for each relaxation mechanism. If the molecular weight is not narrow, the shorter molecules making up the tube will relax fast enough to cause a blurring of the tube. In Chapter 6 we called this *constraint release* and noted that it speeds up the relaxation of a longer molecule in its tube. This results in significant relaxation in what would be the plateau zone for a monodisperse sample of the same polymer.

10.2.1 Large Scale Orientation—The Need for a Finite Strain Tensor

The relaxation processes described above apply to linear viscoelastic behavior. If the deformation is not small or slow, the *orientation* of the chain segments may be sufficiently large to cause a nonlinear response. We will see that this effect *alone* can be accounted for in rheological models by simply replacing the infinitesimal strain tensor by one able to describe large deformations; no new relaxation mechanism needs to be invoked. Nonlinear effects related to orientation, such as normal stress differences, can be described qualitatively in this manner.

10.2.2 Chain Retraction and the Damping Function

In a perfect "step" strain, the deformation is so rapid that no polymer relaxation can occur, and the chain is forced to deform affinely. Unless the strain is very small, this requires the chain to stretch beyond its equilibrium tube contour length, and this gives rise to a new relaxation mechanism, *retraction of the chain within its tube*. (Doi and Edwards [1] call this *contour length relaxation*.) Figure 10.1 illustrates this phenomenon schematically. The chain segment on the left having an initial length of R_1 is stretched affinely by a large strain but then retracts to its original length.

This is a fast relaxation process, and once it is completed, the remainder of the relaxation process occurs as in the case of a linear response, i.e., via reptation. The result is a relaxation modulus curve that has an early, rapid decrease, due to retraction, followed by a curve that has the same shape as that for linear behavior. These features can be seen in Fig. 10.2, which shows relaxation modulus data obtained using several strains for a solution of monodisperse polystyrene with $cM = 5 \cdot 10^5$ [2]. Except at the shortest times and the smallest strains, the modulus curves drop to successively lower levels as the strain is increased. Furthermore, the shear stress versus time curves appear to be superposable by a vertical shift on this log-log plot, again except at quite short times.
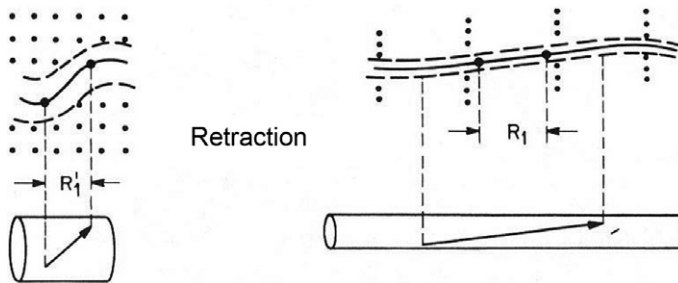
Figure 10.1 Sketch illustrating chain retraction. We see affine deformation of the matrix of constraints (represented by dots) as well as the tube, followed by retraction of the chain within the tube. Affine deformation implies that the microscopic deformation equals the macroscopic strain. After retraction, the chain deformation is non-affine, and the primitive path equals that at equilibrium (drawing from [5]).
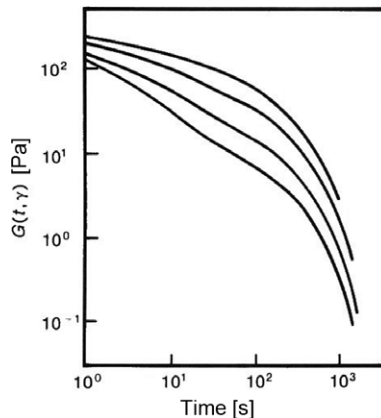
Figure 10.2 Relaxation moduli at several step-strain amplitudes for a polystyrene solution with $cM = 5 \cdot 10^5$ g cm^{-3}. At the smallest strain (top curve), the behavior is linear, but as the strain increases, the modulus is reduced except at very short times (off scale). From Osaki et al. [2].
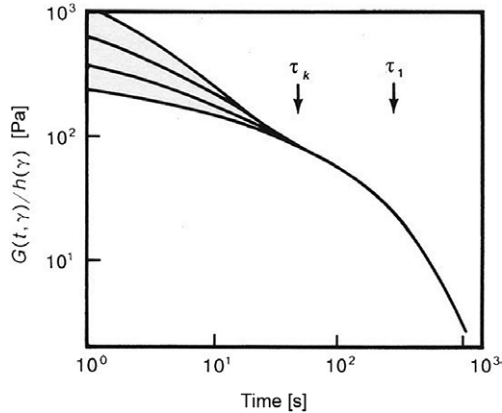
Figure 10.3 Data of Fig. 10.2 replotted as $G(t)/h(\gamma)$. Superposition is achieved by vertical shifting except at times less than τ_k. The longest relaxation time τ_1 is also shown. From Osaki et al. [2].

This implies that the nonlinear relaxation modulus can be separated into time-dependent and strain-dependent factors, as shown by Eq. 10.1.

$$G(t,\gamma) = G(t)\,h(\gamma) \tag{10.1}$$

The data of Fig. 10.2 are replotted in Fig. 10.3 as the ratio $G(t,\gamma)/h(\gamma)$ versus time. At times greater than τ_k the data superpose demonstrating time-strain separability. The value of τ_k was about 30 s in this case, so the duration of the initial ramp was not a problem in the experiments. Also indicated by an arrow is the longest relaxation time. The superposability implies that the nonlinear relaxation modulus can be separated into time-dependent and strain-dependent factors as shown by Eq. 10.1.

This type of stress relaxation is said to exhibit *time-strain separability*, and the factor $h(\gamma)$ is called the *damping function*, which can be thought of as the fraction of the initial stress that is not relaxed by retraction. The behavior of this function for typical melts is discussed in Section 10.4.3, and a quantitative model of the retraction process is described in Chapter 11.

The interpretation of nonlinear stress relaxation using a tube model can be summarized as follows. The small step strain that generates a linear response orients but does not stretch chains. Relaxation then occurs at short times due to equilibration between entanglements within the tube, and at longer times by reptation of the chain out of its tube, with some acceleration of this process due to primitive path fluctuations (contour length fluctuations) (see ref. [1], p. 238). In response to large deformations that cause chain stretch, retraction (contour length relaxation) relaxes the stretch simultaneously with equilibration. Well after the completion of these processes, reptation relaxes the stress arising from the orientation of chain segments in the same way as for small deformations, and the time-dependency of

this final relaxation is therefore the same as in linear viscoelasticity. In this way, the tube-model explains time-strain separability.

10.2.3 Convective Constraint Release and Shear Thinning

We have seen that nonlinear viscoelastic behavior can arise from the orientation of chain segments and from the retraction of the entire chain in its tube. There is one more important new process that can occur, particularly in fast shearing deformations. A serious failure of the original Doi-Edwards theory of nonlinear viscoelasticity (presented in Chapter 11) was its prediction that the shear stress in steady simple shear has a maximum as a function of shear rate. A modification of the model that eliminates this defect was proposed by Marrucci [3] many years later. He proposed a new relaxation mechanism called *convective constraint release* (CCR). (An early version of this idea was proposed in 1965 by Graessley [4].) In steady shear flow, molecules on neighboring streamlines are moving at different speeds, and this carries away entanglements at a rate comparable to the reciprocal of the shear rate. Figure 10.4 illustrates this process schematically. This concept will be used in the interpretation of viscosity data presented later in this chapter. In addition, in steady shear flow this powerful new relaxation mechanism becomes dominant, delaying the onset of chain stretch to shear rates that are generally beyond the limits imposed by flow instabilities and viscous heating in the rheometer.

Convective constraint release strongly suppresses chain stretch in simple shear except at very high strain rates. The degree of stretch depends on the product of the shear rate and a characteristic time governing chain stretch, and this time is expected to be close to the longest Rouse stress relaxation time, τ_R. Since this is often a very small number, and $\dot{\gamma}\tau_R$ must be greater than unity to generate stretch, for many polymers, e.g., linear polyethylene, the shear rate required to generate stretch is not experimentally accessible unless the molecular weight is exceptionally large [4].

a)   b)
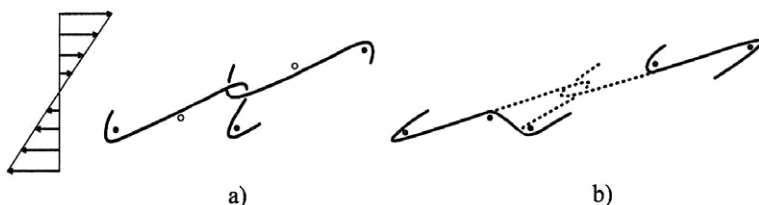
Figure 10.4 Convective constraint release mechanism as envisioned by Ianniruberto and Marrucci. A simple shear field is shown at left and has the effect of sweeping away entanglements originally present in a) allowing the molecules of interest to relax to a new, less constraining entanglement. Filled dots are molecules providing active entanglements; unfilled dots become entanglements after the constraint release.
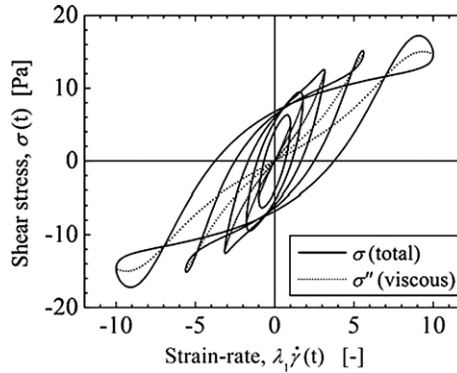
Figure 10.14 Lissajou figures created by plotting shear stress versus Weissenberg number for several levels of nonlinearity. From Ewoldt and McKinley [68].

Ewoldt et al. [69] believe that using Fourier components to characterize nonlinearity fails to reveal important features of the data and propose in its place the use of Chebyshev polynomials, the coefficients of which they use to quantify nonlinear behavior via Lissajous–Bowditch plots. To filter noise, a Fourier transform is first applied to the data, and the data are then reconstructed.

■ 10.7 The Viscometric Functions

If a creep or start-up shearing test is continued until the stresses reach their steady-state values, the rheological response of the material is described completely by three functions of the shear rate. These are the viscosity and the first and second normal stress differences, which were defined by Eqs. 10.29 and 10.30. The three material functions of steady simple shear $\eta(\dot{\gamma})$, $N_1(\dot{\gamma})$, and $N_2(\dot{\gamma})$ are called the *viscometric functions*, and they provide a complete description of the behavior in steady simple shear of an *isotropic* polymer, i.e., one that does not form a liquid crystal or another ordered phase at rest.

10.7.1 Dependence of Viscosity on Shear Rate

Of the viscometric functions, the viscosity is the easiest to measure and the one most often reported. As in the case of Newtonian fluids, the viscosity of a polymer depends on temperature and pressure, but for polymeric fluids it also depends on shear rate, and this dependency is quite sensitive to molecular structure. In particular, the curve of viscosity versus shear rate can be used to infer the molecular weight

distribution of a linear polymer, as is explained in Chapter 8. And in certain cases it can also tell us something about the level of long-chain branching. This curve is also of central importance in plastics processing, where it is directly related to the energy required to extrude a melt.

At sufficiently high shear rates, the viscosity often approaches a power-law relationship with the shear rate. Figure 10.15 is a plot of viscosity versus shear rate for a molten LDPE, and it shows both a low-shear-rate Newtonian region and a high-shear-rate power-law region. This highly branched polymer is valued for the ease with which it can be extruded. This is because the decrease in its viscosity begins at a very low shear rate. This makes the zero-shear viscosity of LDPE very difficult, or impossible, to measure. These data were reported by J. Meissner [70] many years ago but still represent the ultimate in rheometrical technique. He developed a special rheometer to obtain these data.
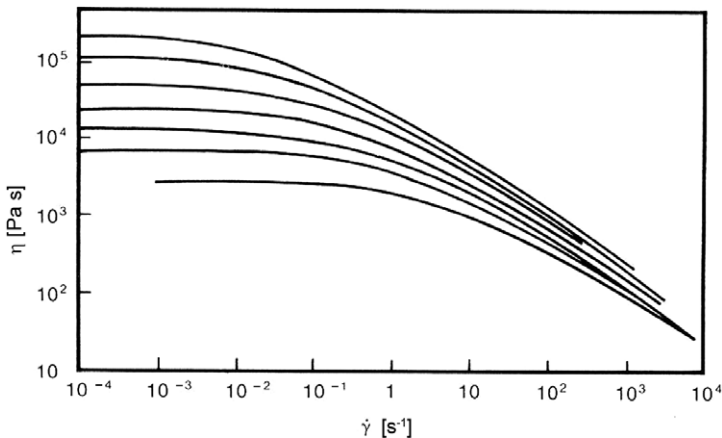
Figure 10.15 Double logarithmic plot of viscosity as a function of shear rate for an LDPE. From top to bottom, the temperatures are: 115, 130, 150, 170 190, 210 and 240 °C. These data were obtained using a specially modified rotational rheometer that made it possible to reach exceptionally low shear rates. From Meissner [70].

10.7.1.1 Empirical Viscosity Models

At the highest shear rates shown in Fig. 10.15, the curves tend toward a linear relationship on the log-log plot, implying that a "power law" can be used to represent the variation of viscosity with shear rate at sufficiently high shear rates, as shown by Eq. 10.56.

$$\eta = k \left(\dot{\gamma} \right)^{n-1} \tag{10.56}$$

It is important to note that this model contains no characteristic time. It thus implies that the power-law parameters are independent of shear rate. Of course such a model cannot describe the low-shear-rate portion of the curve, where the viscosity approaches a constant value. Several empirical equations have been proposed to allow for a transition to Newtonian behavior over a range of shear rates. It was noted in the discussion of the Weissenberg number earlier in this chapter that the variation of η with $\dot{\gamma}$ implies the existence of at least one material property with units of time. The reciprocal of the shear rate at which the extrapolation of the power-law line reaches the value of η_0 is one such characteristic time. Models that can describe the approach to η_0 thus must involve a characteristic time. Examples include the Cross equation [71] and the Carreau equation [72], shown below as Eqs. 10.57 and 10.58 respectively.

$$\eta(\dot{\gamma}) = \eta_0 \left[1 + \left(\lambda \left| \dot{\gamma} \right| \right)^m \right]^{-1} \quad \text{(Cross equation)} \qquad (10.57)$$

$$\eta(\dot{\gamma}) = \eta_0 \left[1 + \left(\lambda \dot{\gamma} \right)^2 \right]^{-p} \quad \text{(Carreau equation)} \qquad (10.58)$$

These models approach power-law behavior at high shear rates, and the dimensionless material constants m and p are simply related to the power law exponent. Hieber and Chiang [73] compared the ability of these two models to fit data for a variety of commercial polymers for purposes of flow simulation. They reported that the Cross equation provided a better fit for the polymers they considered. For more flexibility in fitting data, Yasuda et al. [74] generalized Eq. 10.58 by adding an additional parameter as shown in Eq. 10.59 in order to adjust the curvature in the transition region.

$$\eta(\dot{\gamma}) = \eta_0 \left[1 + \left(\lambda \dot{\gamma} \right)^a \right]^{(n-1)/a} \qquad (10.59)$$

This is often called the Carreau-Yasuda equation.

We note the appearance in these models of a material constant λ with units of time. As mentioned above, such a constant is an essential feature of a rational model for the shear rate dependency of viscosity. Elberli and Shaw [75] compared a number of empirical viscosity equations and found that time constant values obtained by fitting data to two-parameter viscosity models were less sensitive to experimental error than those based on more complex models. The data at low shear rates and in the neighborhood of the reciprocal of the time constant are most critical in obtaining meaningful values of the parameters, while the high shear rate data are important only in regard to the power-law exponent.

Plumley-Karjala et al. [76] evaluated the ability of the models presented above to describe data for a large number of linear and branched metallocene polyethylenes.

They found that the Cross equation gave a good fit to the data and that adding parameters did not lead to a significant improvement. There is no unique procedure for inferring parameter values from data, and different procedures lead to different parameter values. When such equations are fitted to experimental data, information is lost. For example, it is not possible to use such an equation to infer the molecular weight distribution using the methods described in Chapter 8.

Viscosity models are sometimes used to estimate the zero-shear viscosity when no experimental data are available at shear rates sufficiently low that the viscosity is constant. However, this is an unreliable procedure, as there is no fundamental basis for any of these equations, and the resulting value of η_0 should be deemed at best a rough estimate. For example, Kataoka and Ueda [77] found that the Cross equation yielded extrapolated values of η_0 that were about 50% less than measured values.

Graessley [78] suggested that it should be possible to describe the viscosity of all monodisperse, linear, entangled polymers by a single universal curve, if data are plotted as:

$$\frac{\eta}{\eta_0} \quad \text{versus} \quad \eta_0 \, J_s^0 \, \dot{\gamma} \qquad\qquad (10.60)$$

Berry et al. [79] and Attané et al. [80] published generalized plots based on Eq. 10.60.

10.7.1.2 Viscosity Function in Terms of Tube Models

The original Doi-Edwards model predicted that the shear stress in steady shear increases with shear rate from zero and goes through a maximum. This type of behavior has never been observed, and this remained a basic deficiency of tube models until Ianniruberto and Marrucci [81] introduced the concept of *convective constraint release* (CCR). In steady shear flow, molecules on neighboring streamlines are moving at different speeds, and this carries away entanglements at a rate comparable to the reciprocal of the shear rate. An early version of this idea that predates the tube model was presented in 1965 by Graessley [4].

Ianniruberto and Marrucci [81] interpret the variation of viscosity with shear rate for an entangled, linear, monodisperse polymer as follows. At sufficiently slow shear rates, Brownian motion has plenty of time to keep the molecule in its unstressed configuration, so there is no significant orientation and certainly no chain stretch. This is the limiting, slow-flow, linear viscoelastic behavior in which the shear stress is equal to the zero-shear viscosity times the shear rate. As the shear rate increases and approaches the reciprocal of the reptation time, there is a substantial departure from the zero-shear behavior, with the shear stress becoming nearly independent of the shear rate. In this portion of the stress curve, convective constraint release (CCR) is dominant, and as the flow rate is increased, CCR also increases in pro-

This allows for transients in the rate of constraint release during start-up flows: the rate of constraint release builds as the chains stretch in fast flows. Their Rouse "hopping rate" was then set by the rate of constraint release multiplied by a parameter c_v, which is essentially the number of Rouse hops taken by the test chain per tube segment vacated by a matrix chain. This parameter is analogous to the parameter β in the Marrucci formulation of CCR in Eq. 11.15 (which was given the symbol c in the original Marrucci paper [9]).

As noted earlier, the inclusion of CCR in the equations for chain orientation leads to a substantial improvement over the Doi-Edwards and DEMG theories, especially in removing, or greatly reducing, the maximum in shear stress as a function of shear rate. The CCR mechanism, as included in the GLaMM theory and in the earlier theory of Marrucci [9], permits tube segments to disorient somewhat even in intermediate and fast flows, for which $\dot{\gamma} > 1/\tau_d$. This increases the component f_{12} of the tensor $f(s, s')$, leading to a larger shear stress σ than in the absence of CCR. In addition, in fast flows at shear rates comparable to or greater than $1/\tau_s$, the increase in f_{12} leads to an increase in the rate of chain stretch, so that at steady state the chain stretch becomes greater than would be the case without the CCR term. CCR increases chain stretch because the less oriented tube segments can be "gripped" more effectively by the flow. The result, at shear rates comparable to or greater than $1/\tau_s$, is an increase in both the steady-state shear and first normal stress difference. Because of its complexity, and in particular the numerical expense of the two-dimensional space swept out by s and s', the theory of Graham et al. [13] is not very suitable for application to complex flows, even for a monodisperse polymer. However, its most important predictions are captured in a highly simplified toy version of this model, which we present below.

11.3.4 Toy Models Containing CCR and Chain Stretch

11.3.4.1 "Rolie-Poly" Model for CCR

Likhtman, Graham, and McLeish [40, 41] reduced the microscopic theory of Graham et al. [13] to a simplified, one-mode differential toy model, commonly known as the "Rolie-Poly" model (ROuse LInear Entangled POLYmers). In the absence of chain stretch, this may be written in a simple form for tube orientation:

$$\overset{\nabla}{S} = -2(\kappa : S)\,S - \left(\frac{1}{\tau_d} + 2\,\beta\,\kappa : S\right)\left(S - \frac{\delta}{3}\right) \tag{11.16}$$

and the stress is obtained from Eq. 11.11 with the chain stretch set to $\lambda = 1$. This equation is exactly equivalent to Eq. 11.9 for the orientation in the DEMG model, except that a CCR relaxation rate $2\,\beta\,\kappa : S$ has been added, so that the total relaxation

rate is practically identical to Marrucci's original proposal [9] given in Eq. 11.15. β is a constant that is proportional to the parameter c_v of the GLaMM model. This gives a plateau in shear stress at both intermediate and high shear rates.

When chain stretch is added [41], the Rolie-Poly model equation becomes:

$$\overset{\nabla}{\boldsymbol{\tau}} = -\frac{2\left(\lambda - 1\right)}{\lambda\,\tau_{\mathrm{s}}}\,\boldsymbol{\tau} - \left(\frac{1}{\tau_{\mathrm{d}}} + 2\,\beta\,\frac{\left(\lambda - 1\right)}{\tau_{\mathrm{s}}}\,\lambda^{\delta-1}\right)\left(\boldsymbol{\tau} - \boldsymbol{\delta}\right) \tag{11.17}$$

where the stretch, λ is obtained from:

$$\lambda = \sqrt{\frac{\mathrm{tr}\,\boldsymbol{\tau}}{3}} \tag{11.18}$$

and the stress is proportional to the tensor $\boldsymbol{\tau}$:

$$\boldsymbol{\sigma} = G_{\mathrm{N}}^{0}\,\boldsymbol{\tau} \tag{11.19}$$

Equation 11.17 combines both the orientation relaxation and stretch relaxation processes, with separate relaxation times τ_{d} and τ_{s}, in a single, compact, equation. Though it is usual to solve the model in the form of Eq. 11.17, it is instructive to separate the equation out into orientation and stretch components, so that $\boldsymbol{\tau} = 3\,\lambda^{2}\,\boldsymbol{S}$, giving:

$$\overset{\nabla}{\boldsymbol{S}} = -2\left(\boldsymbol{\kappa} : \boldsymbol{S}\right)\boldsymbol{S} - \frac{1}{\lambda^{2}}\left(\frac{1}{\tau_{\mathrm{d}}} + 2\,\beta\,\frac{\left(\lambda - 1\right)}{\tau_{\mathrm{s}}}\,\lambda^{\delta-1}\right)\left(\boldsymbol{S} - \frac{\boldsymbol{\delta}}{3}\right) \tag{11.20}$$

$$\frac{\mathrm{d}\lambda}{\mathrm{d}t} = \lambda\left(\boldsymbol{\kappa} : \boldsymbol{S}\right) - \frac{1}{\tau_{\mathrm{s}}}\left(\lambda - 1\right) - \left(\frac{1}{\tau_{\mathrm{d}}} + 2\,\beta\,\frac{\left(\lambda - 1\right)}{\tau_{\mathrm{s}}}\,\lambda^{\delta-1}\right)\frac{\left(\lambda^{2} - 1\right)}{2\,\lambda} \tag{11.21}$$

The orientation equation Eq. 11.20 is almost identical to the nonstretching equation Eq. 11.16, but the constraint release relaxation rate is now proportional to the rate of stretch relaxation $\left(\lambda - 1\right)/\tau_{\mathrm{s}}$. This respects the physical situation that release of constraints is caused by the *retraction* of chain ends through the entanglement mesh, which is caused by stretch relaxation. The stretch equation Eq. 11.21 may be compared to Eq. 11.10: it contains a (usually negligible) contribution from the orientation relaxation time, but also a contribution from CCR, reflecting the fact that constraint release relaxes both orientation and stretch. A similar relaxation term for chain stretch is present in the model proposed by Mead, Larson, and Doi [35].

The Rolie-Poly model gives qualitatively correct predictions in all three regimes: slow flow $(\dot{\gamma} \leq 1/\tau_{\mathrm{d}})$, intermediate flow $(1/\tau_{\mathrm{d}} \leq \dot{\gamma} \leq 1/\tau_{\mathrm{s}})$, and fast flow $(\dot{\gamma} \geq 1/\tau_{\mathrm{s}})$. The parameter β controls the level of CCR and the exponent δ controls the effect of chain stretching on the rate of CCR. (Note that the symbol δ is here a scalar exponent, and

is not the unit tensor $\boldsymbol{\delta}$.) A negative value of δ leads to suppression of CCR when the chain is stretched and therefore to larger overshoots in shear stress and first normal stress difference during start-up of steady shear. Likhtman and Graham [41] set $\delta = -1/2$ and $\beta = 0.5$, the latter corresponding roughly to $c_v = 0.05$. These choices of the two parameters β and δ make the simplified theory match more exactly the predictions of the full theory. The theory is also readily extended to multiple modes, merely by assigning a new equation to each new relaxation mode. The constants G_N^0 and $\tau_{d,i}$ for each mode i are obtained by fits to linear viscoelastic data. Often, only one stretch relaxation time $\tau_{s,1}$ for the first (longest) mode needs to be assigned, since the higher modes have stretch times fast enough to be assumed instantaneous; for these modes, Eq. 11.17 reduces to Eq. 11.16. The predictions of the multi-mode version of this model for start-up of steady shear will later be compared to experimental data for an entangled polybutadiene solution (in Fig. 11.7).

It is possible to modify the Rolie-Poly model to include finite extensibility, simply by increasing both the stress $\boldsymbol{\sigma}$ and rate of retraction $(\lambda - 1)/\tau_s$ by the factor $k_s(\lambda)$ introduced in Eq. 11.13.

11.3.4.2 Differential Model of Ianniruberto and Marrucci

All of the above differential equations suffer the defect that even under slow-flow conditions the second normal stress difference is zero. This defect is eliminated in a CCR constitutive equation of Ianniruberto and Marrucci [37], referred to as the "double constraint release with chain stretch" (DCR-CS) model:

$$\tau = \frac{1}{2\left(1/\tau_d + |\boldsymbol{\kappa} : \boldsymbol{S}|\right)} + \tau_s \tag{11.22}$$

$$\overset{\nabla}{\boldsymbol{S}^2} + 2\,\boldsymbol{S}^2\left(\boldsymbol{\kappa} : \boldsymbol{S}\right) + \frac{2}{\tau}\,\boldsymbol{S}\left(\boldsymbol{S} - \frac{1}{3}\boldsymbol{\delta}\right) = 0 \tag{11.23}$$

$$\frac{d\lambda}{dt} = \lambda\,\boldsymbol{\kappa} : \boldsymbol{S} - \frac{1}{\tau_s}\left[k_s'(\lambda)\,\lambda - 1\right] \tag{11.24}$$

$$\boldsymbol{\sigma} = G_N^0\,k_s'(\lambda)\,\lambda^2\,\boldsymbol{S} \tag{11.25}$$

$$k_s' = \frac{\lambda_{max} - 1}{\lambda_{max} - \lambda} \tag{11.26}$$

Equations 11.22 to 11.25 are the counterparts to Eqs. 11.9 to 11.11 of the DEMG theory, or of Eqs. 11.19 to 11.21 of the Rolie-Poly model. The most significant difference between these equations is the form of the orientation equation, Eq 11.23.

Subject Index